On More than Two Decades of Celestial Reference Frame VLBI Observations in the Deep South: IVS-CRDS (1995 - 2021)

Publications of the Astronomical Society of Australia (2023), **40**, e041, 22 pages
doi:10.1017/pasa.2023.33

CAMBRIDGE UNIVERSITY PRESS

Research Article

On more than two decades of Celestial Reference Frame VLBI observations in the deep south: IVS-CRDS (1995–2021)

S. Weston[1]*, A. de Witt[2]*, Hana Krásná[3], Karine Le Bail[4,5], Sara Hardin[6], David Gordon[6], Shu Fengchun[7], Alan Fey[6,5], Matthias Schartner[8], Sayan Basu[2], Oleg Titov[9], Dirk Behrend[4], Christopher S. Jacobs[10], Warren Hankey[11], Federico Salguero[12] and John E. Reynolds[13]

[1]Institute for Radio Astronomy & Space Research (IRASR) School of Engineering, Computer and Mathematical Sciences Faculty of Design and Creative Technologies, Auckland University of Technology, Auckland, New Zealand, [2]The South African Radio Astronomy Observatory, Cape Town, South Africa, [3]Department für Geodäsie und Geoinformation, Technische Universität Wien (TU Wien), Wien, Austria, [4]NVI, Inc. at NASA Goddard Space Flight Center, Greenbelt, MD, USA, [5]Chalmers University of Technology/Onsala Space Observatory, Onsala, Sweden, [6]U.S. Naval Observatory, Washington, DC, USA, [7]Shanghai Astronomical Observatory, Chinese Academy of Sciences, Shanghai, China, [8]ETH Zürich, Institute of Geodesy and Photogrammetry, Zurich, Switzerland, [9]Geoscience Australia, Canberra, ACT, Australia, [10]Jet Propulsion Laboratory, California Institute of Technology, Pasadena, CA, USA, [11]University of Tasmania, Hobart, Australia, [12]National Scientific and Technical Research Council, Argentina (CONICET), Buenos Aires, Argentina and [13]CSIRO Space and Astronomy, Australia Telescope National Facility, Epping, NSW, Australia

Abstract

The International VLBI Service for Geodesy and Astrometry (IVS) regularly provides high-quality data to produce Earth Orientation Parameters (EOP), and for the maintenance and realisation of the International Terrestrial and Celestial Reference Frames, ITRF and ICRF. The first iteration of the celestial reference frame (CRF) at radio wavelengths, the ICRF1, was adopted by the International Astronomical Union (IAU) in 1997 to replace the FK5 optical frame. Soon after, the IVS began official operations and in 2009 there was a significant increase in data sufficient to warrant a second iteration of the CRF, ICRF2. The most recent ICRF3, was adopted by the IAU in 2018. However, due to the geographic distribution of observing stations being concentrated in the Northern hemisphere, CRFs are generally weaker in the South due to there being fewer Southern Hemisphere observations. To increase the Southern Hemisphere observations, and the density, precision of the sources, a series of deep South observing sessions was initiated in 1995. This initiative in 2004 became the IVS Celestial Reference Frame Deep South (IVS-CRDS) observing programme. This paper covers the evolution of the CRDS observing programme for the period 1995–2021, details the data products and results, and concludes with a summary of upcoming improvements to this ongoing project.

Keywords: VLBI; IVS; Geodesy

(Received 17 March 2023; revised 31 May 2023; accepted 2 June 2023)

1. Introduction

Very Long Baseline Interferometry (VLBI) is a collaborative and cooperative endeavour involving many individuals and institutions around the world. Part of this cooperation and collaboration, using VLBI observations of extragalactic radio sources to conduct geodesy and astrometry, has been formalised under the umbrella of the International VLBI Service for Geodesy and Astrometry (Nothnagel et al. 2017), which has organised this cooperation over the past 23 years. The IVS provides products derived from the analysis of VLBI data to the scientific community, of which some of the main products are:

1. Accurate measurements of station positions and velocities which contribute significantly to the realisation of the International Terrestrial Reference Frame (ITRF, Altamimi et al. 2021), in particular to the definition of its scale
2. Accurate measurements of the angular positions of extragalactic radio sources which define and realise the International Celestial Reference Frame (ICRF, Charlot et al. 2020)
3. The five daily Earth orientation parameters (EOP, Eubanks 1993), including Earth rotation parameter *UT1-UTC* and nutation which are provided uniquely, which provides the link between the ICRF and the ITRF

The ICRF is a catalogue of positions of extragalactic radio sources with the highest precision, which are crucial to many applications. For example, the ICRF provides sources that are observed in the geodetic VLBI observations conducted by the IVS to measure the orientation of Earth in space and station motions (Hellmers et al. 2021), which in turn contributes to the realisation of the ITRF and allows studies of the motion of the tectonic plates and the interior of the Earth (Carter and Robertson 1993), and measurements of the ionosphere and troposphere which allows for atmospheric studies (Heinkelmann et al. 2011). High-accuracy celestial reference frames (CRFs) are also crucial for many other applications such as satellite tracking, orbit determination, and

Corresponding author: S. Weston; Email: sweston@aut.ac.nz

Cite this article: Weston S, de Witt A, Krásná H, Le Bail K, Hardin S, Gordon D, Fengchun S, Fey A, Schartner M, Basu S, Titov O, Behrend D, Jacobs CS, Hankey W, Salguero F and Reynolds JE. (2023) On more than two decades of Celestial Reference Frame VLBI observations in the deep south: IVS-CRDS (1995–2021). *Publications of the Astronomical Society of Australia* **40**, e041, 1–22. https://doi.org/10.1017/pasa.2023.33

*S. Weston and A. de Witt are joint first authors

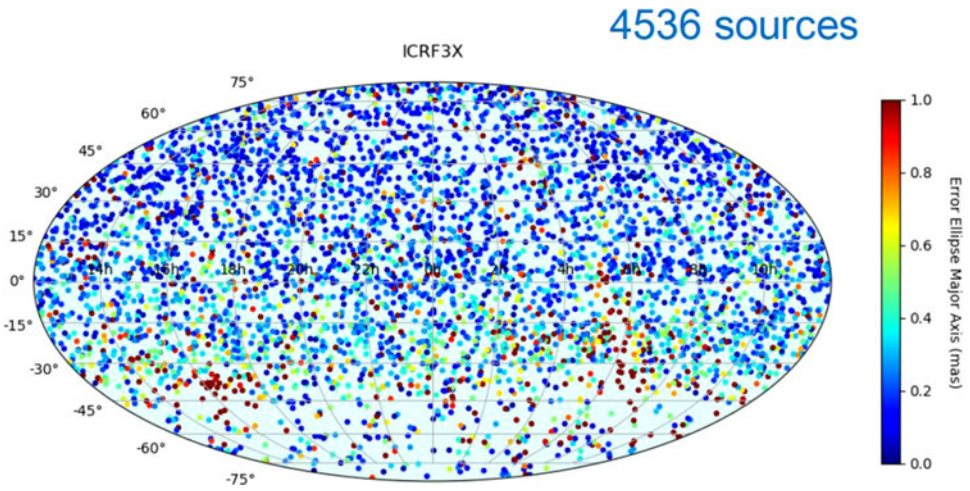

Figure 1. The ICRF3-SX (2018) has 4536 sources, but quite clearly the number of sources become sparse below a declination of −30° (Charlot et al. 2020).

deep-space navigation (Thornton and Border 2000), alignment of the planetary ephemerides (Park et al. 2021), studies of special and general relativity (Fomalont et al. 2009) such as Galacto-centric acceleration (MacMillan et al. 2019), and for phase-referencing observations in astronomy (Beasley and Conway 1995; Rioja and Dodson 2020).

The first iteration of the ICRF (ICRF1, Ma et al. 1998) was based on positions of 608 extragalactic radio sources, of these a subset of 212 sources uniformly distributed on the sky were identified as 'defining sources', and served to define the axes of the reference frame. This iteration used data obtained through VLBI observations at the standard geodetic and astrometric *S*/*X*-band (2.3/8.4 GHz) frequencies. The ICRF1 was adopted by the International Astronomical Union (IAU) as the new fundamental CRF in 1997, and replaced IAU's Fundamental Catalogue FK5 (Fricke et al. 1988), which was based on optical observations of galactic stars. The IVS began operations in 1999, and coordinated continued *S*/*X*-band observations and improvements on the original ICRF. As a result a second iteration, the ICRF2 (A. L. Fey et al. 2015) with 3414 sources of which 295 are defining sources, was adopted by the IAU in 2009 and officially replaced the ICRF1 on 2010 January 01. Since the first release of ICRF, the ongoing observing programmes run by the IVS together with other specific independent projects have ensured the continued expansion of the VLBI database, and as such a third iteration, the ICRF3 (Charlot et al. 2020) was adopted by the IAU in 2018 (see Resolution B2[a]) and replaced the ICRF2 on 2019 January 01. The ICRF3 is based on nearly 40 years of data and contains *S*/*X* positions of 4536 extragalactic sources, including 303 uniformly distributed defining sources. The ICRF3 has a noise floor of 30 as, with median position uncertainties at *S*/*X*-band of about 127 as in right ascension (RA) and 218 as in declination—more than a factor of three improvement over the ICRF2. In addition, the ICRF3 added two complementary catalogues at *K*-band (24 GHz) and *X*/*Ka*-band (32 GHz), making it the first multi-wavelength frame ever realised. Since ICRF3 there have been many dedicated efforts to further improve the CRF at radio wavelengths, and current CRF solutions (de Witt, Jacobs, and Gordon 2022; Gordon, deWitt, and Jacobs 2022).

Catalogues of compact radio sources, including the ICRF3, are generally weaker in the South by factors of 2 or more in both density and precision (deWitt, Jacobs, and Gordon 2022). This is because the stations contributing to geodetic and astrometric VLBI observations have an uneven distribution between the hemispheres, currently ∼80% of the stations are in the Northern Hemisphere and ∼20% of the stations are in the Southern Hemisphere. As a result, and despite the significant improvements over its predecessor, the ICRF3 still has deficiencies by factors of 2–3 in the South (Charlot 2018; Charlot et al. 2020). In addition, the deficit of long North-South baselines in the ICRF3 contributes to the Declination (Dec) precision being a factor of two or more worse than the RA precision. The distribution of the ICRF3 *S*/*X*-band sources on a projection of the celestial sphere clearly shows the decrease in the number of sources and the number of observations per source for sources below −30° Dec, and shows that Southern sources have generally less precise positions (Charlot et al. 2020) (see Fig. 6 reproduced here in Fig. 1[b]). When looking at a world map of all 167 antennas (situated on 126 different sites) that participated in the observations used for ICRF3 (see Fig. 1[c] in Charlot et al. 2020), the uneven distribution of antennas between the hemispheres is very apparent. Of those 167 antennas, only 14 antennas contributed from the Southern Hemisphere. The plots in Fig. 2 show the number of observations for North-only, South-only, and North–South baselines for all astrometric and geodetic VLBI observations between 1980 April and 2021 June. The plot clearly shows the disparity between the number of Northern and Southern observations, with only ∼20% of the observations coming from North–South baselines and only ∼10% from all Southern baselines.

The Southern Hemisphere also suffers from a lack of dedicated imaging campaigns to map and monitor the structure of individual ICRF sources. Many ICRF sources exhibit spatially extended intrinsic structure that may vary with time and frequency. It is

[a]See Resolution B2 at https://iau.org/static/resolutions/IAU2018_ResolB2_English.pdf.

[b]https://www.aanda.org/articles/aa/full_html/2020/12/aa38368-20/F6.html.
[c]https://www.aanda.org/articles/aa/full_html/2020/12/aa38368-20/F1.html.

https://doi.org/10.1017/pasa.2023.33 Published online by Cambridge University Press

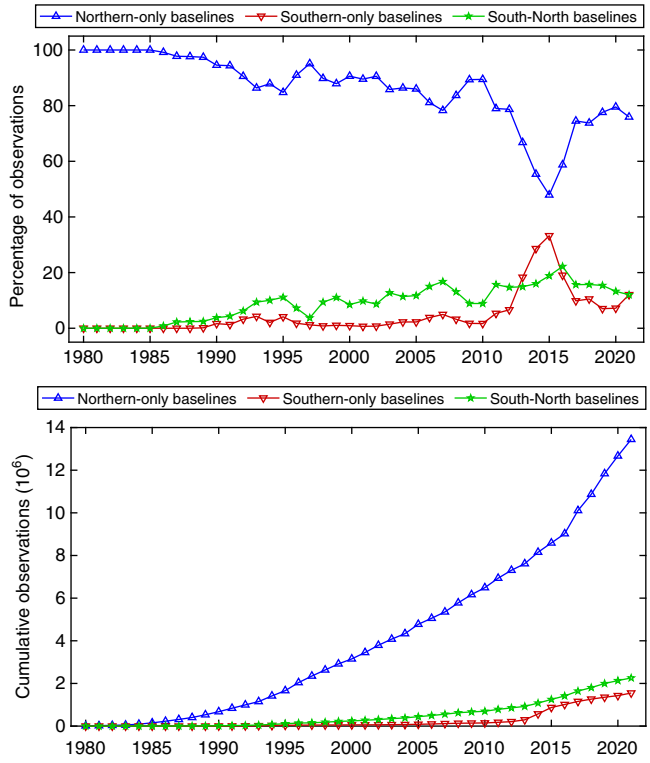

Figure 2. The plot on the top shows the percentage of astrometric and geodetic VLBI observations for the period April 1980 to June 2021 June on Northern only (blue), Southern only (red), and North–South (green) baselines. The plot on the bottom shows the cumulative totals for the same baselines over the same period.

well known that source structure can introduce significant errors in the geodetic and astrometric VLBI delay measurements and instabilities in the individual source positions (Charlot 1990; Gattano, Lambert, & Le Bail 2018; Xu et al. 2019). It is therefore important to map the structures of these sources on a regular basis to assess the astrometric source suitability and to track the source structure variations over time. There have, however, only been a few imaging sessions of ICRF sources in the South (Hungwe et al. 2011; Petrov et al. 2019) and dedicated campaigns to map and monitor source structure have proven difficult to obtain. Nevertheless, recent investigations to image source structure from existing astrometric and geodetic observations in the South have shown that dedicated imaging campaigns, as are done in the North, may indeed be possible (Basu et al. 2016; Basu, deWitt, & Gattano 2021).

Since its inception, the IVS has initiated and coordinated many observing programmes intended to provide astrometric observations useful in improving and densifying the CRF. Dedicated Southern Hemisphere astrometric programmes proved most successful in providing and maintaining the fundamental Southern Hemisphere reference frame for the ICRF. In particular, the Celestial Reference Frame Deep South (CRF-DS) observing sessions were initiated in 1995 and became the IVS-CRDS observing programme in 2004 (henceforth called CRDS). The CRDS programme aims to provide astrometric VLBI observations of sources in the deep South for improving and densifying the ICRF, and in recent years it has also contributed to the imaging and monitoring of source structure.

This paper provides the details and evolution of the CRDS observing programme for the period 1995 June–2021 December, as well as details on the data products and results. Section 2 provides a timeline overview of the evolution and major developments of the CRDS observing programme from the early sessions that started in 1995 June up to 2021 December. In Section 3 we discuss the methods employed in detail. This consists of the participating networks and stations (Section 3.1), source selection (Section 3.2), and scheduling strategies (Section 3.3). Details of the data correlation, analysis, and data products are provided in Section 3.4. A discussion about the CRDS observing programme results to date and remarks are given in Section 4. This consists of the astrometric results (Section 4.1) and imaging results (Section 4.2), and finally an overview of the network performance (Section 4.3). A final discussion of the CRDS programme to date and future plans to improve the observing programme to further densify and strengthen the Southern CRF are discussed in Section 5.

2. Detailed CRDS observing timeline

This section provides an overview of the evolution and major developments of the CRDS observing programme from the early sessions that started in 1995 June up to 2021 December. Details include the network coverage and participating stations over this period, as well as any improvements and changes in the frequency sequence, data rates, and scheduling strategies.

2.1. From 1995 June (CRF-DS1) to 2010 December (CRDS49)

The CRDS sessions started with two sessions each in 1995 and 1996. The first 9 sessions in this initial period were called CRF-DS1 to CRF-DS9. There was a gap of 7 years until 2003 then some 45 sessions were run between 2003 and 2008 (CRF-DS5 to CRDS49). These early sessions were scheduled by the United States Naval Observatory (USNO). Most were single-baseline sessions between the HartRAO 26-antenna in Hartebeesthoek, South Africa and the Hobart 26-m antenna in Tasmania, Australia, but a few included other stations, such as the Parkes 64-m antenna in New South Wales, Australia and the Deep Space Station 45 (DSS45) in Tidbinbilla, Australia. These early sessions made significant contributions to ICRF2, being almost the only sessions to add new Southern sources. There were no CRDS sessions in 2009 or 2010 because the HartRAO 26-m antenna suffered a major bearing failure and was down for more than 2 years for repairs.

2.2. From 2011 March (CRDS50) to 2017 May (CRDS88)

In the late 2000s a group of three new 12-m VLBI antennas (Yarragadee 12-m, Katherine 12-m, and Hobart 12-m), called the AuScope array (Lovell et al. 2013), were commissioned by the University of Tasmania in Australia. An identical antenna, the Warkworth 12-m, was also commissioned in Warkworth, New Zealand (Gulyaev and Natusch 2010). Between 2011 July and 2012 November (CRDS52-61), one or two at a time of these 12-m antennas were scheduled in the CRDS sessions. The two sessions before 2011 July (CRD50-51) consisted of single-baseline observations between the HartRAO 26-m and Hobart 26-m antenna. In 2013 all four 12-m antennas were added to the CRDS observing programme. Very importantly, this increased the number of regular CRDS stations from 2 to 6, and also allowed a greater cadence of source observing within a 24-h geodetic or astrometric VLBI session due to the much faster slew speeds of the 12-m antennas. Between 2013 January and 2017 May, twenty-six CRDS sessions

https://doi.org/10.1017/pasa.2023.33 Published online by Cambridge University Press

were observed (CRDS62-CRDS88), of which thirteen had the full six-station network, seven had five stations participating, and six sessions observed with only 4 stations. The CRDS53 and CRDS61 sessions also included the Parkes 64-m antenna, and the CRDS58 session included the Deep Space Station 43 (DSS43) 70-m antenna in Tidbinbilla, Australia. Up to CRDS65 the data recording rate was 128 Mbps, but in 2013 July (CRDS-66) the recording rate was increased to 256 Mbps.

Imaging of sources from CRDS sessions data started in 2013 January (CRDS-63), to analyse source structure and variability, and to update flux catalogues in the South (see Section 4.2).

2.3. From 2017 July (CRDS89) to 2019 March (CRD101)

To be fully compliant with the VLBI Global Observing System (VGOS, Petrachenko et al. 2013), the Hobart 12-m antenna was upgraded with a new wide-band cooled receiver (2–14 GHz), and in 2017 July (CRDS-89) it was removed from the CRDS programme. Between 2017 July and 2019 March (CRD101), thirteen CRDS sessions were observed of which eleven included all of the remaining five stations. The CRDS94 session also included the HartRAO 15-m antenna. In 2017, a Southern Hemisphere astrometry group, later formalised under the IVS as the Southern VLBI Operations Centre (SVOC, Behrend 2018; deWitt, Nickola, et al. 2019) was formed, with the aim to improve and densify the *S*/*X*-band CRF in the South. This group adopted the following measures over this period to improve the final data products:

1. Increased sensitivity of Southern sessions for detection of weaker sources down to ≈350 mJy or less.
2. Increased the data rate of Southern sessions by a factor of 8, from 128 Mbps to 1 Gbps.
3. Optimised scheduling of Southern sessions to allow for simultaneous astrometric and imaging observations.
4. Included mapping and monitoring of source structure in analysis to quantify non-point-like structure.
5. Improved precision of Southern source positions by a factor of 2.5.
6. Expanded the Southern source list by a factor of 2.
7. Improved the sky coverage of Southern sources.
8. Improved overlap with higher frequency radio CRFs and Gaia optical CRF.

As a result, many improvements were made to the CRDS sessions (de Witt, Le Bail, et al. 2019). From 2018 January (CRDS93), the data recording rate was increased from 256 Mbps to 1 Gbps and the frequency sequence was optimised to avoid radio frequency interference (RFI, see Section 3.1) in particular at *S*-band. In addition the scheduling was improved and the source list was expanded (see Section 3.2) with optimisation for both astrometry and imaging (see Section 4).

2.4. From 2019 May (CRD102) to 2021 July (CRD113)

In 2019 May (CRD102) the O'Higgins 9-m antenna in Antarctica was added to the CRDS programme, and in 2019 June (CRD103), the Katherine 12-m antenna was upgraded for VGOS observations and removed. In 2020 February (CRD105) the Aggo 6-m antenna in Argentina was added to the CRDS network. Between 2020 February (CRD105) and 2021 May (CRDS112), eight CRDS sessions were observed, of which half had five participating stations, and the other half had six stations. In 2021 July (CRD113) the Hobart 26-m antenna was temporarily removed from the CRDS observing programme due a bearing failure, and remains out of service at the time of writing this paper. Subsequently, the CRDS113 session was observed with only four stations. The loss of the Hobart 26-m antenna, being one of only two large antennas in the CRDS network (the other being the HartRAO 26-m), has severely impacted the success rate of the CRDS sessions (see Section 4).

2.5. From 2021 August (CRD114) to 2021 December (CRD116)

In 2020 the IVS-CRF Committee[d] was formalised, also incorporating the SVOC, to make recommendations to the IVS Directing Board on observing programmes and strategies for the *S*/*X*-band CRF (Behrend 2019, 2020). The charter[e] for the IVS-CRF Committee was accepted by the IVS Directing Board on 2020 October 14. In 2021 the IVS-CRF Committee made recommendations to add the 25-m Very Long Baseline (VLBA) antennas in Mauna Kea (VLBA-MK) and Saint Croix (VLBA-SC), as well as the 50-m Kunming antenna in China, to the CRDS observing programme. In 2021 August (CRD114) the two VLBA antennas were added to the CRDS schedule forming a seven-station network, and in October and 2021 December (CRD115 and CRD116) the 50-m Kunming antenna was also added forming an eight-station network. Unfortunately, the VLBA stations observed with a wrong LO value for *S*-band channels and the baselines between the VLBA stations and other antennas could not be correlated. Since then, test observations with a revised *S*-band setup for the VLBA stations were successful, and VLBA-MK and VLBA-SC will be added to future CRDS sessions.

3. Methods

This section details the methods employed in the CRDS programme, starting with the setup of the observing network, source selection, scheduling strategies, correlation, and finally the analysis undertaken to produce the final data products.

3.1. Observing networks and setup

The early CRDS sessions consisted of mostly single-baseline observations between the HartRAO and Hobart 26-m antennas, occasionally including a few other antennas. From 2011 onward, more stations were added to the CRDS sessions and between 2011 July and 2019 March the CRDS programme, for the most part, including the following six stations: HartRAO 26-m (Hh), Hobart 26-m (Ho), Hobart 12-m (Hb), Katherine 12-m (Ke), Yarragadee 12-m (Yg), and Warkworth 12-m (Ww), recalling that Hb was removed from the CRDS programme in 2017 July. Two of these sessions also included the Parkes 64-m antenna (Pa), while the HartRAO 15-m antenna (Ht) and DSS43 Tidbinbilla 70-m antenna (Ti) each participated in a single session. In 2019 May the O'Higgins 9-m antenna (Oh) was added to the CRDS programme and in 2019 June Ke was removed. In 2020 February the AGGO 6-m antenna (Ag) was added to the CRDS network. In 2021 July (CRDS113) Ho was temporarily removed from the CRDS observing programme due to a bearing failure and in 2021 October the 50-m Kunming

[d] https://ivscc.gsfc.nasa.gov/about/com/crfc/index.html.
[e] https://ivscc.gsfc.nasa.gov/about/com/crfc/crfc_charter.pdf.

https://doi.org/10.1017/pasa.2023.33 Published online by Cambridge University Press

Table 1. The eleven participating CRDS VLBI stations, with their geocentric coordinates used in the session schedule files. The last three entries are the stations added very recently.

Station code	Station name	Station geocentric coordinate XYZ (m)			Solution (Epoch)
Ag	Aggo 6-m, Observatorio Argentina-Alemán de Geodesia (AGGO), Argentina	2765116.70	−4449233.81	−3626420.56	2020c
Hb	Hobart 12-m, University of Tasmania, Australia	−3949990.58	2522421.17	−4311708.24	2011b
Hh	HartRAO 26-m, Hartebeesthoek, South Africa	5085442.79	2668263.49	−2768697.04	GLB1069
Ho	Hobart 26-m, University of Tasmania, Australia	−3950236.74	2522347.56	−4311562.55	GLB1069
Ht	HartRAO 15-m, Hartebeesthoek, South Africa	5085490.80	2668161.48	−2768692.62	2013
Ke	Katherine 12-m, University of Tasmania, Australia	−4147354.59	4581542.40	−1573303.30	2011b
Oh	O'Higgins 9-m, ERS/VLBI Station O'Higgins, Antarctica	1525833.48	−2432463.71	−5676174.48	2020c
Pa	Parkes 64-m, CSIRO, Australia	−4554232.05	2816758.99	−3454035.88	GLB1069
Ti	70-m Tidbinbilla (DSS-43), CSIRO, Australia	−4460894.39	2682361.29	−3674747.98	GLB1069
Ww	Warkworth 12m, AUT University, New Zealand	−5115324.39	477843.30	−3767192.88	2011b
Yg	Yarragadee 12m, University of Tasmania, Australia	−2388896.06	5043349.97	−3078590.92	2011b
Mk	Manua Kea VLBA Station, Hawaii, USA	−5464075.28	−2495247.63	2148297.61	2020c
Sc	St Croix VLBA Station, St Croix, USVI	2607848.71	−5488069.47	1932739.83	2020c
Km	Kunming 40m, Yunnan Astronomical Observatory, China	−1281153.12	5640864.43	2682653.37	2020c

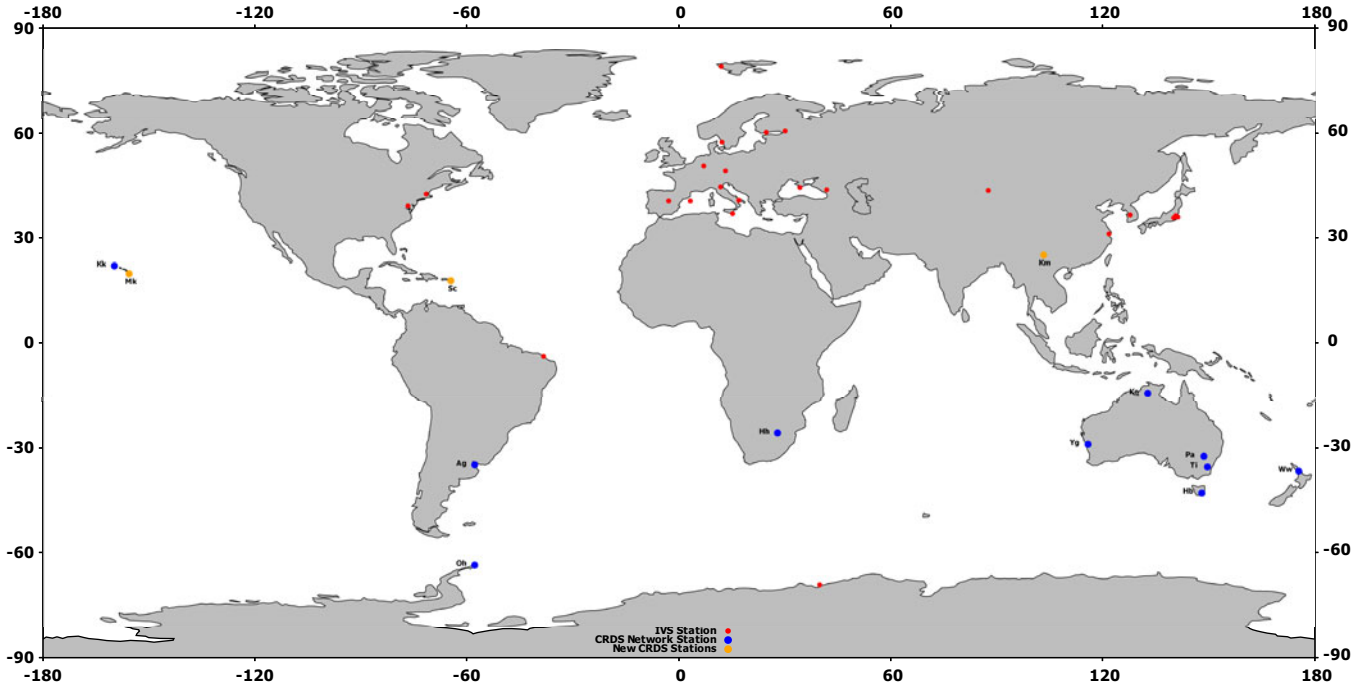

Figure 3. Network map showing IVS and cooperating stations (in red) and stations that participated in the CRDS programme during the last decade (in blue and orange). Hobart hosts two stations separated by a few hundred metres, so Hb on this figure represents both Hb and Ho. This is also true for Hartebeesthoek where Hh represents both Hh and Ht.

antenna (Km) was added. In 2021 August the VLBA-MK (Mk) and VLBA-SC (Sc) antennas were added, but the data from these two antennas could not be correlated with other stations due to a mismatch in the *S*-band frequency setup. Details of the fourteen IVS VLBI stations that participated in CRDS sessions between 2011 July and 2021 December, are listed in Table 1. The full IVS station network is shown in Fig. 3, highlighting the stations that participated in the CRDS sessions during this period. Note that all the stations used for CRDS sessions are IVS stations, except for Ti.

Between the first observations in 1995 and the last session included in this paper (2021 December, CRD116) the CRDS programme observed a total of 116 sessions. Between 2011 March and 2021 December, 67 CRDS sessions were observed and these were scheduled roughly once every 2 months—giving six sessions per year, except for 2012 in which seven sessions were scheduled. Each of these sessions was 24-h in duration and had between 2 and 8 scheduled stations, with an average of 5 stations per session. It is important to note that not all scheduled stations necessarily

https://doi.org/10.1017/pasa.2023.33 Published online by Cambridge University Press

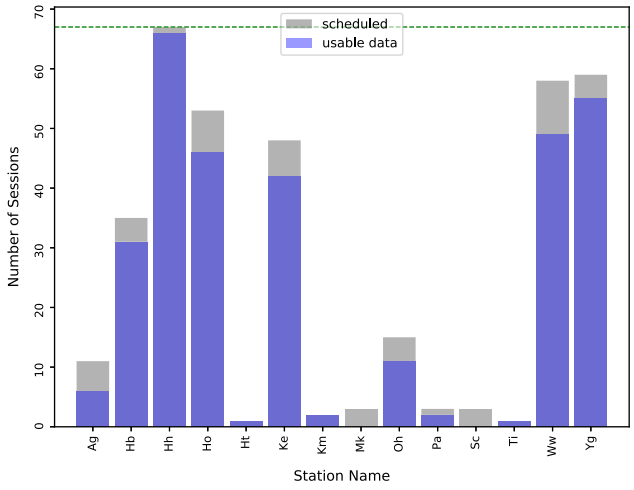

Figure 4. The total number of scheduled sessions by station for the 2011–2021 period (in grey), and the number of sessions for which an antenna had usable data (in light blue). The dashed green line shows the total number of sessions observed (67) for the 2011–2021 period.

participated or delivered usable data over the entire 24-h session, due to various technical issues and outages (see Section 4.3). A summary of the number of sessions each station was scheduled in versus the number of sessions it participated in and had usable data for, during the 2011–2021 period, is shown in Fig. 4. It can be seen that the faster slewing 12-m antennas (Hb, Ke, Yg and Ww) have taken over the bulk of observing enabling a significant increase in the sources observed within a 24-h period.

The CRDS sessions are all dual-band (*S*/*X*) observations, the *S*-band is a selection of frequencies from 2.2-2.3 GHz and *X*-band is a selection from 8.2-8.9 GHz. Ionosphere corrections are computed from the delay differences between the two bands S and X, these are then applied to the *X*-band solution for the final data product. Data is recorded in 14 intermediate frequency (IF) bands, consisting of eight *X*-band (+2 side-bands) and six *S*-band IFs. Up to 2013 May (CRDS65) the data was recorded with 16×4 MHz bands at 1-bit, resulting in a data recording rate of 128 Mbps. From 2013 July (CRDS66) the bands were increased to 8 MHz doubling the recording rate to 256 Mbps. In 2018 January (CRDS93) the data recording rate was increased again, from the 256 Mbps (16 × 8 MHz bands, 1-bit recording) to 1 Gbps (16 × 16 MHz bands, 2-bit recording) and a total bandwidth of 256 MHz. However, the VLBA antennas can only record a total bandwidth of 128 MHz (4 × 16 MHz *S*-band and 4× 16 MHz *X*-band IF's). The CRDS frequency sequence was also optimised in 2018 January, mainly to avoid RFI. Test observations using different frequency setups were conducted to choose the best. In 2021 August (CRD114) the frequency sequence was updated again, to both accommodate the VLBA antennas and to avoid high side lobes and RFI.

3.2. Source selection

Between 2011and 2017 the sources observed in the CRDS sessions were primarily the 76 ICRF2 defining sources South of −30° Dec. The ICRF2 defining sources were known to be strong ($\gtrsim$500 mJy) and relatively compact. Given the CRDS data rates during this time (128 Mbps and later 256 Mbps) they provided a pool of sufficiently bright sources detectable on even the longest baselines. In addition, there were also 20 ICRF2 non-defining sources that were observed in 2011 (CRDS51-53 and CRDS55). Towards the end of 2017, it was decided to revisit the strategy and review the CRDS programme, in particular to expand the CRDS source list. At this point, other IVS programmes had also started contributing to Southern observations, which added many more observations of sources in the South. These included, for example, the AUSTRAL (AUA, Plank et al. 2017) sessions that started in 2011 and the Asia-Oceania VLBI group for Geodesy and Astrometry (AOV, McCallum, Wakasugi, & Shu 2019) sessions which started in 2015. It was therefore decided to use the CRDS programme to re-observe all CRF sources South of −15° Dec and to give priority to sources observed in fewer than 10 sessions in order to improve the accuracy of the source positions in both coordinates (de Witt, Le Bail, et al. 2019; de Witt et al. 2021). Subsequently, in 2017 November (CRDS92) ten additional bright ICRF2 non-defining sources, one of which was also observed in 2011 (CRDS53), were added to the CRDS schedule.

In 2018 January (CRDS93) the CRDS data rate was increased to 1 Gbps giving a factor of two increase in sensitivity. This allowed for weaker sources, down to ∼350 mJy given an integration time of 6 min, to be included in the schedules. A list of 216 CRF sources South of −15° Dec with $\leq$ 10 observing sessions and with flux densities ∼350 mJy were added to the CRDS programme. This list was revised as updated CRF solutions became available. A few bright *K*-band and *X*/*Ka*-band CRF sources that were not in the *S*/*X*-band frame (∼20 sources) were also added to the schedule. The 2018 March (CRDS94) session, by request of the ICRF3 Working Group, was dedicated to observing a list of 31 potential ICRF3 defining sources South of −40° Dec. These 31 sources had only a few observations and no available images, and thus additional observations were required ahead of finalising the ICRF3 catalogue. These observations were repeated for the 2018 August and September (CRDS97 and 98) sessions. From 2021 May (CRD112) onwards, following recommendations from the IVS-CRF committee, only ICRF3 defining sources South of −15° Dec were observed in the CRDS sessions in order to re-assess their suitability as defining sources in preparation for an ICRF4. The sessions between 2018 and 2021 (CRDS93–116) added an additional 237 sources to the CRDS programme.

Between 2011 March and 2021 December (CRDS50–116) a total of 342 sources were observed in the CRDS sessions, including 104 of the 114 ICRF3 defining sources South of −15° Dec. From these observations 298 sources (101 ICRF3 defining sources) were successfully detected to give a detection rate of 87 %. Fig. 5 shows the distribution of the CRDS sources used as defining sources in ICRF3 on a Mollweide projection of the celestial sphere, using a heat colour scale to show the number of sessions and the number of observations per source with the blue being the lesser and the red being the greater. Fig. 6 depicts all the CRDS detected sources on a Mollweide projection of the celestial sphere, again using a heat colour scale to show the number of sessions and the number of observations per source. The number of sessions per source ranges between 1 and 35, with an average of 8 sessions and 156 observations per source. The complete source list for the 2011–2021 period is provided in Appendix 1, where ICRF3 defining sources have been identified.

3.3. Scheduling strategies

Between 2011 and 2017 the schedules for the CRDS sessions were usually prepared by the USNO with some by NASA Goddard

https://doi.org/10.1017/pasa.2023.33 Published online by Cambridge University Press

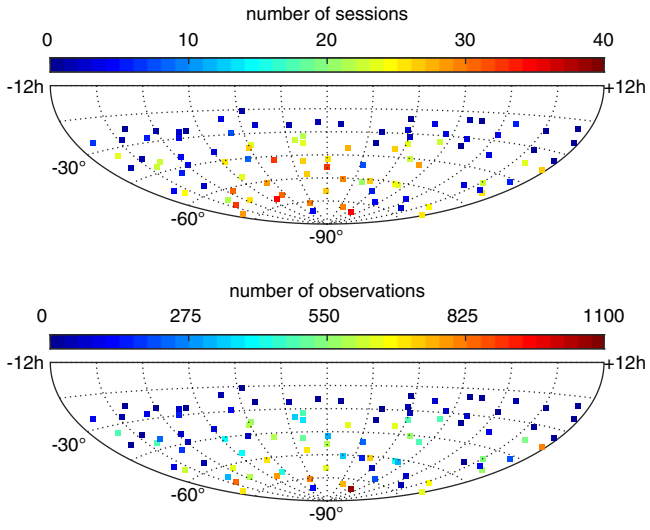

Figure 5. The top plot shows the ICRF3 defining sources with a Mollweide projection using a heat colour scale (on the right hand side) for the points to show the number of sessions each source was observed in, with the blue end being the least and red being the greater. The bottom plot shows the ICRF3 defining sources, also using a heat colour scale for the points to show the number of observations for each source. Both plots are for sessions CRDS50-116.

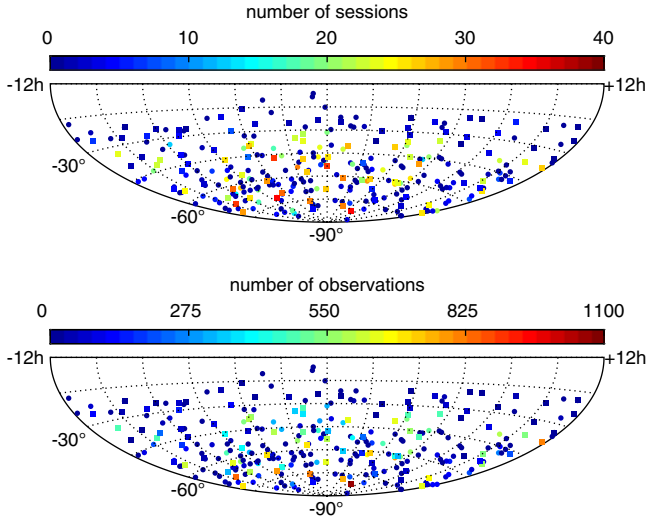

Figure 6. The top plot shows all the sources with a Mollweide projection using a heat colour scale for the number of sessions per source (ICRF3 sources are squares and other sources are circles). The bottom plot shows the same sources, using a heat colour scale for the number of observations per source (ICRF3 sources are squares and other sources are circles). Both plots are for sessions CRDS50-116.

Space Flight Center (GSFC), using the geodetic VLBI scheduling software sked (Vandenberg 1997). These sessions were all scheduled using a fixed scan length that ranged between 360 and 600 s except for CRDS58 which used a scan length of 120 s, and between 2 and 7 antennas were scheduled per session. This allowed for an average of 38 sources, 147 scans, and 1337 observations to be scheduled per session. The number of scans per source per session ranged between 1 and 14, with an average of 4 scans per source. Although the minimum number of stations per scan was set to two, which is standard for geodetic and astrometric VLBI type schedules, those sessions with four or more antennas had on average 89% of the scans observed by four or more antennas. This made them more suitable for imaging which requires at least four stations per scan and preferably three or more scans per source.

In 2018 January the CRDS scheduling was optimised to allow for both astrometry and imaging, and from 2018 January (CRDS93) to 2019 March (CRD101) the CRDS schedules were prepared at HartRAO using the astronomical VLBI scheduling programme sched (Walker 2018). The changes that were made to the scheduling approach included the following: (1) using the full network of stations when possible for every scan, with no subnetting as is used routinely for geodesy schedules; (2) observing at least 3–8 scans per source spread evenly over Hour Angle (HA) range to allow for optimal u,v-coverage for imaging without compromising the astrometric goals of the experiment; (3) including blocks with tropospheric calibrators that are also used as astrometric ties and as calibrators for imaging; and (4) scheduling sessions as part of a campaign rather than individually, to ensure that each source in the list will receive the required amount of observing time. These sessions had between 4 and 6 antennas and used a fixed scan length that ranged between 180 and 300 s for calibrator scans (∼20 ICRF2 defining sources that were added to each session), and 300 s for target scans (∼30 new sources that were added to each schedule). This allowed for an average of 49 sources, 227 scans, and 1962 observations to be scheduled per session. The number of scans per source per session ranged between 1 and 8, with an average of 4.7 scans per source. The minimum number of stations per scan was set to four or higher, depending on the number of participating antennas.

Fig. 7 shows the u,v-coverage plots for source 0302-623 and the improvement obtained starting with CRDS63 (2014 Jan) where the source was observed with 4 stations and in 4 scans, CRD100 (2019 Feb) with 5 stations but in only 2 scans and CRD102 (2019 May) where the source was observed with 6 stations and in 6 scans. This improvement in u,v-coverage has resulted in better imaging; important for all sources but far more important for monitoring and selecting ICRF defining sources. An example is 0302-623 which was an ICRF2 defining source, but due to the improved imaging was deselected as an ICRF3 defining source because of the source structure as seen in Fig. 12.

From 2019 June (CRD102) the CRDS schedules were prepared at TU Wien using the VieSched++ (Schartner and Böhm 2019) geodetic VLBI scheduling software. The VieSched++ software has the capability to produce VLBI astronomical-type schedules by using a source-centric scheduling approach with special constraints for imaging (as listed in the previous section). This was done by defining individual minimum repeat times per source, representing the minimum time between two scans to the same source. The minimum repeat times were calculated based on the time the source was visible by at least four stations and a target number of scans, which was typically between five and eight. The source selection was done iteratively as discussed in Schartner and Böhm (2019). Therefore, the initial source list was divided into a calibrator source group and a target source group. After each session, the initial source list was updated and the observed target sources were removed to have a proper rotation among all sources. Since the participating antennas had quite different characteristics, such as slew speeds and sensitivities, long idle times existed for some stations. To reduce these idle times and increase the Signal to Noise Ratio (SNR), the station observing times per scan were extended in case of available idle time.

https://doi.org/10.1017/pasa.2023.33 Published online by Cambridge University Press

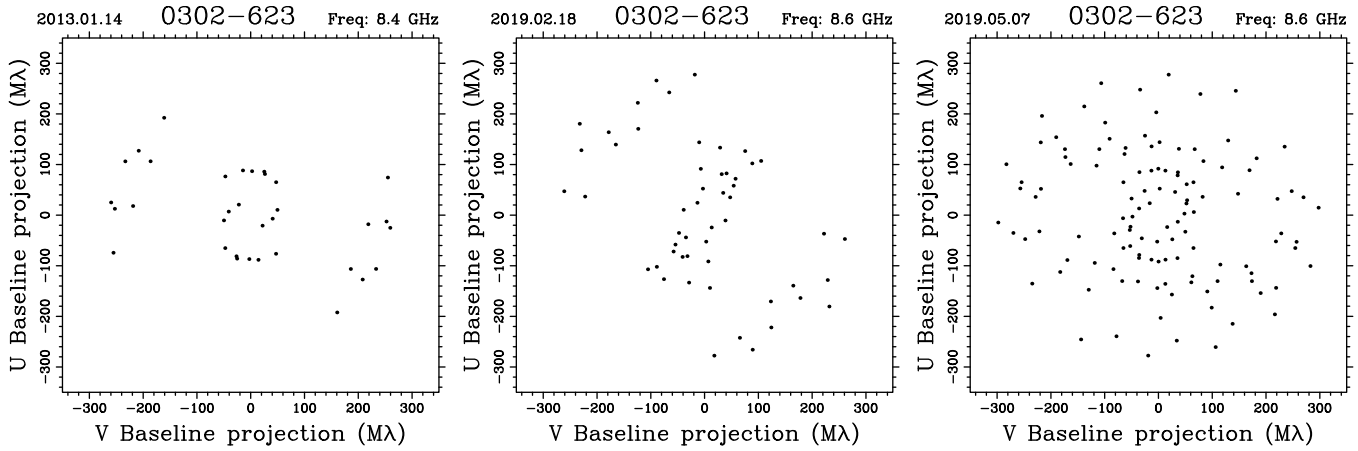

Figure 7. The *u*,*v*-coverage plots for source 0302-623 (left to right) for session CRDS63 (2013 January), CRD100 (2019 February) and for CRD102 (2019 May).

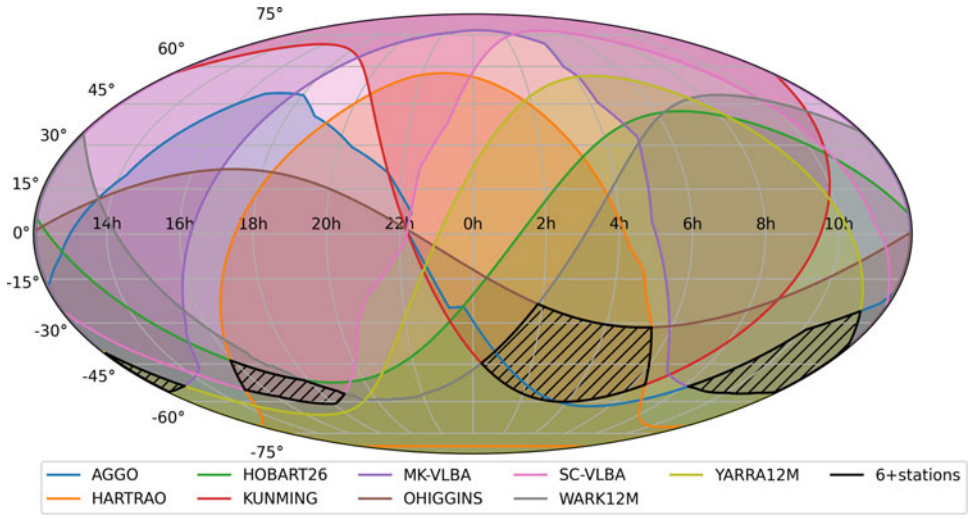

Figure 8. Sky visibility per station as a function of right ascension and Dec for the CRD115 network after applying the local horizon mask and a cut-off elevation of 5 degrees. Areas visible by six or more stations are hatched in black.

Another significant challenge was the very inhomogeneous and sparse station network. As an example, the commonly visible sky for the 2021 October (CRD115) network is displayed in Fig. 8. Areas of the highest interest, e.g. where a source can be observed by six or more stations, are highlighted with a hashed black area. It can be seen that no commonly visible sky exists between Mk and Hh and Sc and Yg, while the commonly visible sky between Km and Ag is also very small. Together, all these requirements pose significant constraints on the scheduling. To find a proper balance between these constraints, the VieSched++ multi-scheduling feature was used to test several different optimisation combinations. Out of this pool of possible schedules, the best one was selected and distributed.

Another challenge with the CRDS scheduling is that source flux information is often not available or not reliable. Therefore, the sessions between 2019 May (CRD102) and 2020 September (CRD110) used a fixed integration time of 280 s per scan. However, due to the high number of non-detections, SNR-based scheduling using the sked-catalogue parameters (Vandenberg 1997) was used for the 2021 May and August (CRD112 and 113) sessions. Finally, this was changed to a strategy where the sources were divided into three groups based on their brightness and were observed in either 240, 360, or 480 sec scans. On average, the sessions scheduled with VieSched++ (between 2019 May, CRDS102 and 2021 December, CRDS116) included between 6 and 8 antennas, which allowed for an average of 36 sources, 201 scans, and 2165 observations to be scheduled per session. The number of scans per source per session ranged between 1 and 10, with an average of 5.7 scans per source. The schedules from the earlier sessions in this period had 95% or more of the scans observed by four or more stations, while CRD114–116, which included Km, Mk, and Sc, had only ∼ 70% of the scans observed by 4 or more stations.

Finally, Figs. 9 and 10 show the overall CRDS scheduling statistics for the period 2011–2021. It is clear from these plots that, in general, the number of scheduled sources and scans per session, as well as the average number of scans per source and average number of observations per baseline, all increased from 2018 (CRDS93). However, the number of sources scheduled per session shows a decrease from 2019 May (CRD102), as both the integration time per scan and the number of scans per source were

https://doi.org/10.1017/pasa.2023.33 Published online by Cambridge University Press

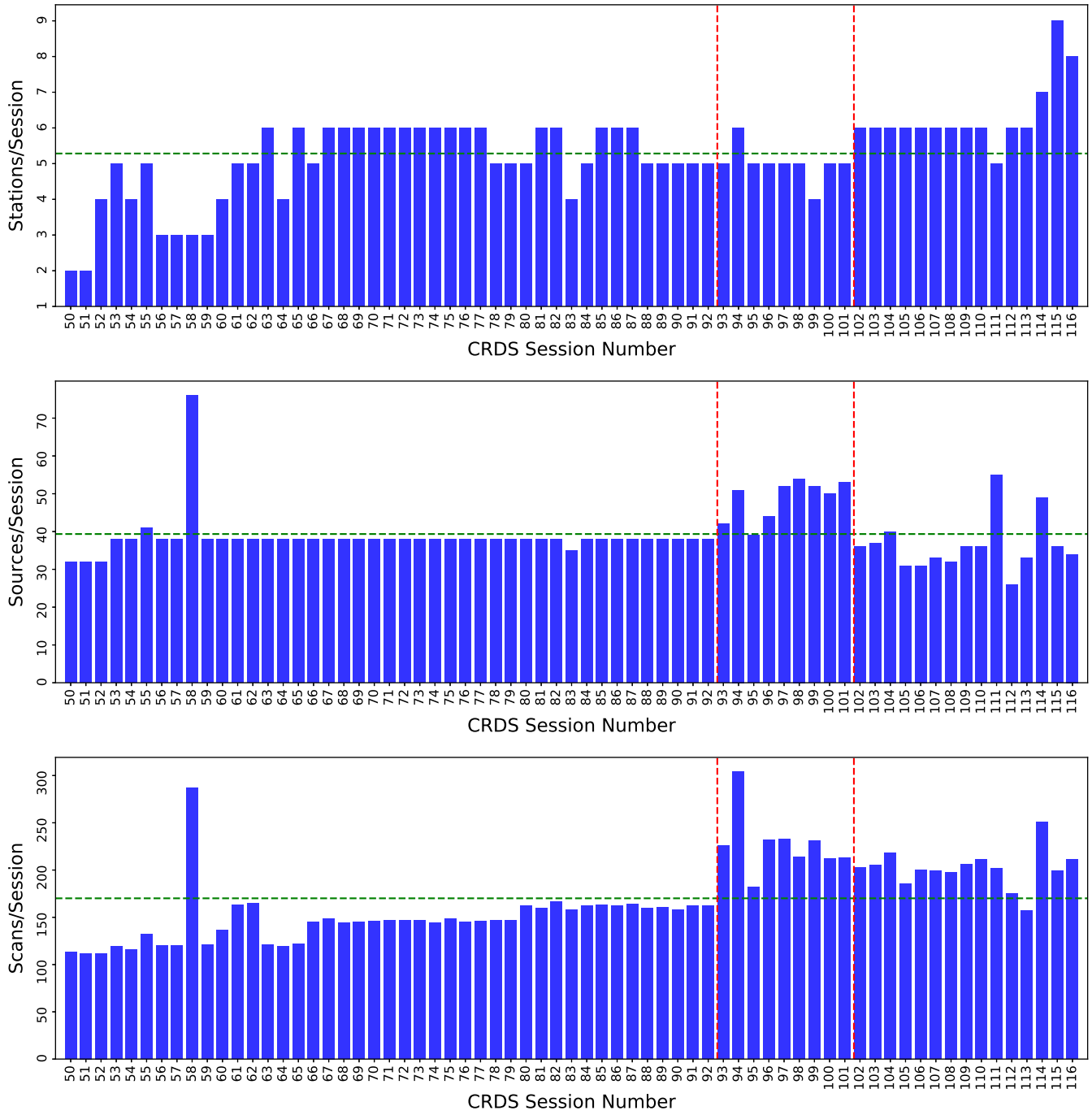

Figure 9. Scheduling statistics for the CRDS sessions between 2011 and 2021 (CRDS50–116) showing the number of stations (top plot), the number of sessions (middle plot), and the number of scans (bottom plot). The red dashed vertical lines indicate the time frames when different scheduling software were used, and the green dashed horizontal lines show the average of the distribution.

increased, allowing for fewer sources to be scheduled. The increase in the integration times was mainly due to the decrease in the sensitivity of the network at the time, owing to the loss of two of the larger and more sensitive antennas, Ke and Ho, and the addition of the smaller less sensitive antennas, Ag and Oh. The rapid decrease in the number of observations per baseline seen for the last three sessions is a result of the additional scheduling constraints imposed by the three Northern antennas (Km, Mk, and Sc) that were added to the network. It should be noted that the statistics and plots provided in this section purely reports on the numbers obtained from the scheduling and does not reflect the actual number of participating antennas nor the success rate of the observations themselves, which are discussed in Section 4.

3.4. Correlation, analysis, and data products

The raw antenna data for all stations was usually correlated at the USNO using their VLBI Correlator facility. Prior to 2014 October,

https://doi.org/10.1017/pasa.2023.33 Published online by Cambridge University Press

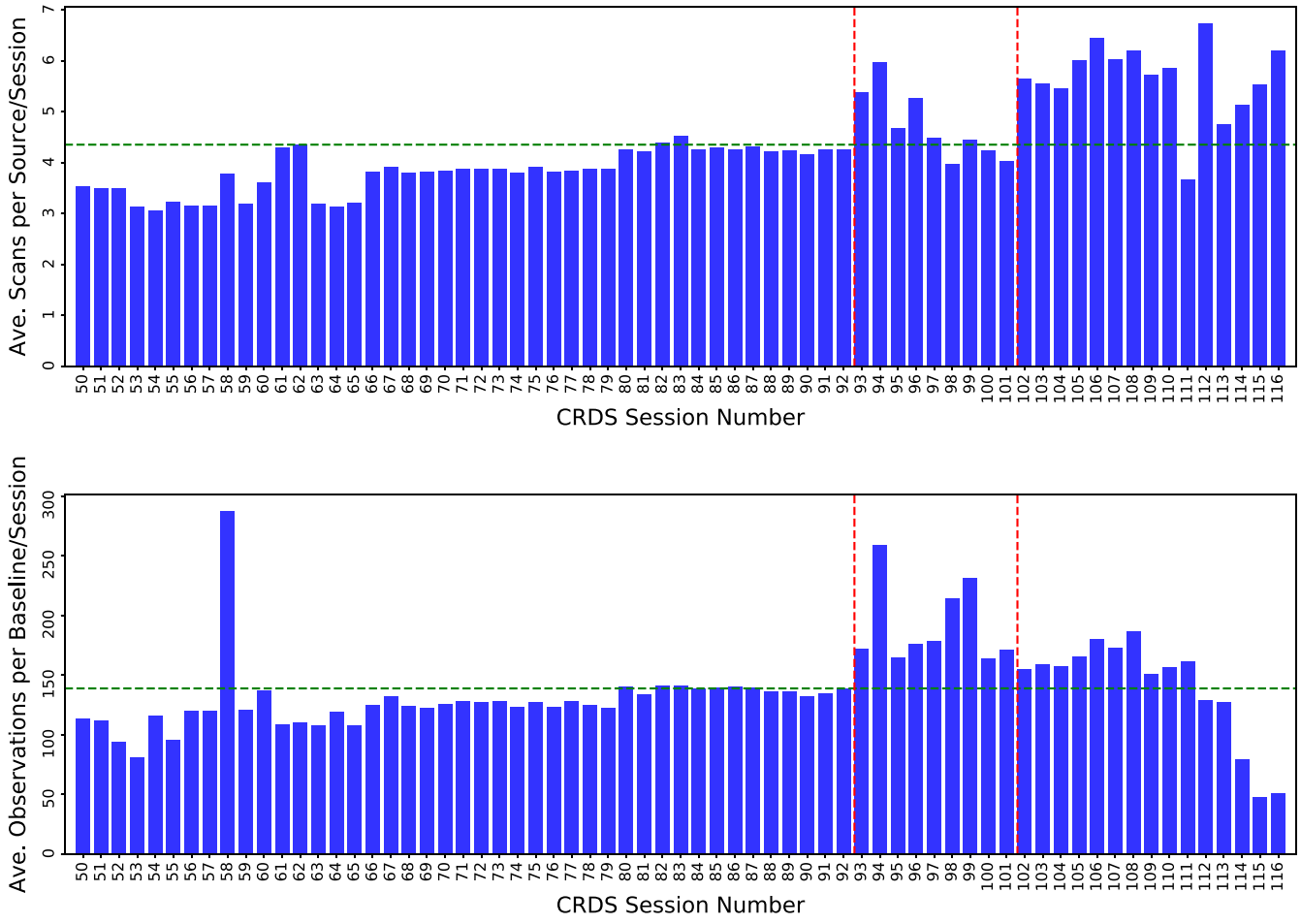

Figure 10. Scheduling statistics for the CRDS sessions between 2011 and 2021 (CRDS50–116), showing the average number of scans per sources (top plot), and the average number of observations per baselines (bottom plot), for each session. The red dashed vertical lines indicate the time frames when different scheduling software were used, and the green dashed horizontal lines show the average of the distribution.

this was done on the Mark IV hardware correlator. In 2014 USNO transitioned to the DiFX (Deller et al. 2011) software correlator (A. Fey et al. 2010; Hall and Veillette 2015). First, the raw data was correlated with the DiFX software package. Visibilities are produced and converted to the Mk4 format for post-processing and the fits format for imaging. When necessary, station clock models are adjusted to reduce single-band delay residuals and the data are re-correlated. The CRDS82, 84, 86, 88, 90, 92, and 93 sessions were correlated with the Shanghai DiFX software correlator (Shu et al. 2018) that is hosted and operated by the Shanghai Astronomical Observatory (SHAO) of the Chinese Academy of Sciences (CAS).

After correlation with DiFX, fringe fitting was performed with the Haystack Observatory Post-processing Software, hops (MIT Haystack Observatory 2021). In cases where RFI degrades the fringe amplitude for a significant number of scans, the affected channels were removed. Fringes were also inspected to ensure that there was a strong phase calibration signal. Stations such as Ho and Ww had no initial phase calibration and required an artificial one applied with hops. Once significant RFI was removed and all stations have phase calibrations, the data was sent to the IVS Data Centres in the vgosDB format. However, the turnaround of the correlation of the CRDS sessions was severely affected by the arrival time of data from the Oh antenna. Since there is no high-bandwidth data connectivity to Antarctica and the Oh station, data was recorded onto hard disks and these are transported on an irregular basis when supply ships depart. Analysis of all of the CRDS sessions was done at both USNO and GSFC. The analysis begins by computing theoretical delays using the Calc programme (Charlot et al. 2020) and and inserting them into the database. Then meteorological data (surface pressures, temperatures, and humidities) and phase cal cable calibration data (if available) is added. Individual sessions were initially analysed with programme solve (Ma 1978) in the interactive mode until the 2018/2019 time frame, and then with νSOLVE (Bolotin et al. 2014) as it was gradually phased in. The interactive analysis first involves finding and resolving the 2π group delay ambiguities in both X and S bands and creating the ionosphere-free X/S combination. Various parameters are then solved for in a least-squares solution, such as piece-wise continuous clock and residual atmosphere terms at typically 60-min intervals, tropospheric gradients over the entire session, antenna positions, and occasionally the coordinates of new sources. Three-sigma editing is performed and lastly the database is updated. Further analysis is then done on multiple databases with a global VLBI analysis package, such as calc/solve (Ma 1978) or various other analysis packages within IVS

https://doi.org/10.1017/pasa.2023.33 Published online by Cambridge University Press

(IVS 2021). The global solutions can involve dozens or thousands of databases and solve for both global parameters (one value for the entire data span) and arc parameters (separate values for each database). Global parameters usually are the station positions, station velocities, and source positions. Arc parameters are usually the piece-wise continuous clock and residual atmosphere terms (typically at 60 or 30 min intervals), tropospheric gradients (typically at 6 h intervals), and the five EOPs (X and Y polar motion, UT1, and dX and dY nutation). A solve batch solution of the 57 available CRDS sessions from 2011-2021 shows that there were ∼41,000 individual baseline observations at 11 sites and that 261 sources were observed in multiple sessions.

The databases created from the correlation and analysis as well as auxiliary data, such as schedule files and station log files, are stored in three primary IVS Data Centres (see the Data Availability Statement).

4. Results and performance

The primary purpose of the CRDS programme is astrometry, in particular to maintain and improve the *S*/*X*-band CRF in the Deep South. In recent years there have also been efforts to obtain imaging results from the CRDS sessions in order to assess the astrometric suitability of the CRF sources in the South, in particular those sources for which no images were available. Additionally, the CRDS sessions like all other IVS sessions contribute to the realisation of the terrestrial reference frame. They are included in the Quarterly combination of 24-h IVS sessions[f] computed by the BKG/DGFI-TUM Combination Centre which releases the estimated TRF as an official IVS product (Bachmann et al. 2021). They are used for the station coordinate estimation but are not used for EOP determination. The USNO Quarterly solution to date uses CRDS59,69,71 & 91 in their EOP Solution.[g] Furthermore, the current realisation of the International Terrestrial Reference Frame ITRF2020 (Altamimi et al. 2022), includes all available CRDS sessions at that time, i.e., until CRD105. Details of the astrometric and imaging results obtained from the CRDS sessions are provided in the following sections, Sections 4.1 and 4.2. The overall performance of the CRDS sessions is discussed in Section 4.3

4.1. Astrometric results

The early CRDS sessions from 1995 June (CRF-DS1) to 2010 December (CRDS49) made significant contributions to the ICRF2, being almost the only sessions to add new Southern sources. The CRDS sessions between 2011 (CRDS50) and 2017 (CRDS92) primarily observed the 76 ICRF2 defining sources South of −30° Dec, and this long-term monitoring provided precise positions for the ICRF2 defining sources in the deep-South. From 2018 (CRDS93) additional sources were added to the CRDS programme, as detailed in Section 3.2, in particular CRF sources South of −15° Dec observed in fewer than 10 sessions and the ICRF3 defining sources.

The 2022 April *S*/*X* astrometric solution from the USNO (e.g. sx-usno-220422, Gordon, de Witt, and Jacobs 2022) which includes all of the CRDS sessions up to 2021 December (CRD116), shows significant improvement over the ICRF3. However, the number of sources is still more than a factor of 3 less in the far-South (≤−45°) compared to the far-North (≥45°), with 269 sources in the far-South and 881 sources in the far-North. While the average number of sessions per source in the far-South is only a factor of 1.8 less than in the far-North, the average number of observations per source is more than a factor of 3 less in the far-South, with an average of 131 observations per source in the far-South and 449 in the far-North. The median formal uncertainties are a factor of 1.2 weaker in *RA* cos (*Dec*) in the far-South and a factor of 1.6 weaker in *Dec*, showing that much work is still needed in the far-South.

In order to measure the impact of the more recent CRDS observations (2018 January, CRDS93–2021 December,CRD116), we compare the 2022 April *S*/*X* astrometric solution (sx-usno-220422) to a solution where we exclude all CRDS sessions from 2018 January (CRDS93) onward. The 2022 April astrometric solution includes 266 sources that were observed and detected in CRDS sessions between 2018 and 2021, but for this comparison, we consider only the 182 of those sources that are in the far-South. Fig. 11 shows the number of sessions and number of observations, as well as the *RA* cos (*Dec*) and *Dec* uncertainties from the 2022 April *S*/*X* astrometric solution (sx-usno-220422) for each of the 182 sources, with and without the CRDS sessions. The median number of sessions per source increases from 8 to 11, when CRDS sessions are included, and the number of observations increases by a factor of 1.5. The median uncertainties are a factor of 1.2 lower in *RA* cos (*Dec*) and 1.4 lower in *Dec*, when the CRDS sessions are included in the solution. Thus, the CRDS sessions have significantly improved the precision of the 182 sources observed in the far-South since 2018.

4.2. Imaging results

A campaign to image CRF sources in the deep-South using the CRDS sessions started in 2013 January (Basu et al. 2016), and the imaging of twelve CRDS sessions (CRDS63, 66, 68, 94, 95, 96, 97, 98, 100, 101, 102, and 103) has been completed to date (Basu et al. 2018; Basu, deWitt, and Gattano 2021). Imaging of the older sessions, prior to CRDS93, was challenging because of poor sensitivity and poor *u*,*v*-coverage, and for this reason only three of these sessions were imaged. CRDS93 was not imaged as it had no usable data for Hh which provides the long baselines, and CRDS99 was not imaged as it had only three participating stations.

The correlated visibility data was calibrated with the NRAO's Astronomical Imaging Processing System (aips, Greisen 2003). The data were first split into single-frequency (*S*- and *X*-band) files and each band was then calibrated separately using the standard calibration and editing steps and utilities available in aips. Data for sessions prior to CRDS93 were not available in Flexible Image Transport System (fits) file format for use in aips, and an interface programme called mk4in (Alef and Graham 2002) was used to import the raw mkiv correlator data into aips and then convert and export it into fits format. This process was carried out at the Bonn correlator. Amplitude calibration, in general, has been a challenge, since system temperature (T_{sys}) and gain curve information is not readily available for IVS sessions. The T_{sys} and gain curve information had to be extracted from the respective session log files, and for some stations nominal values had to be used as no T_{sys} was

[f]https://ivscc.gsfc.nasa.gov/IVS_AC/ITRF2020/itrf2020_sx_sessionTable_v2021Feb10.txt.

[g]https://crf.usno.navy.mil/quarterly-vlbi-solution.

https://doi.org/10.1017/pasa.2023.33 Published online by Cambridge University Press

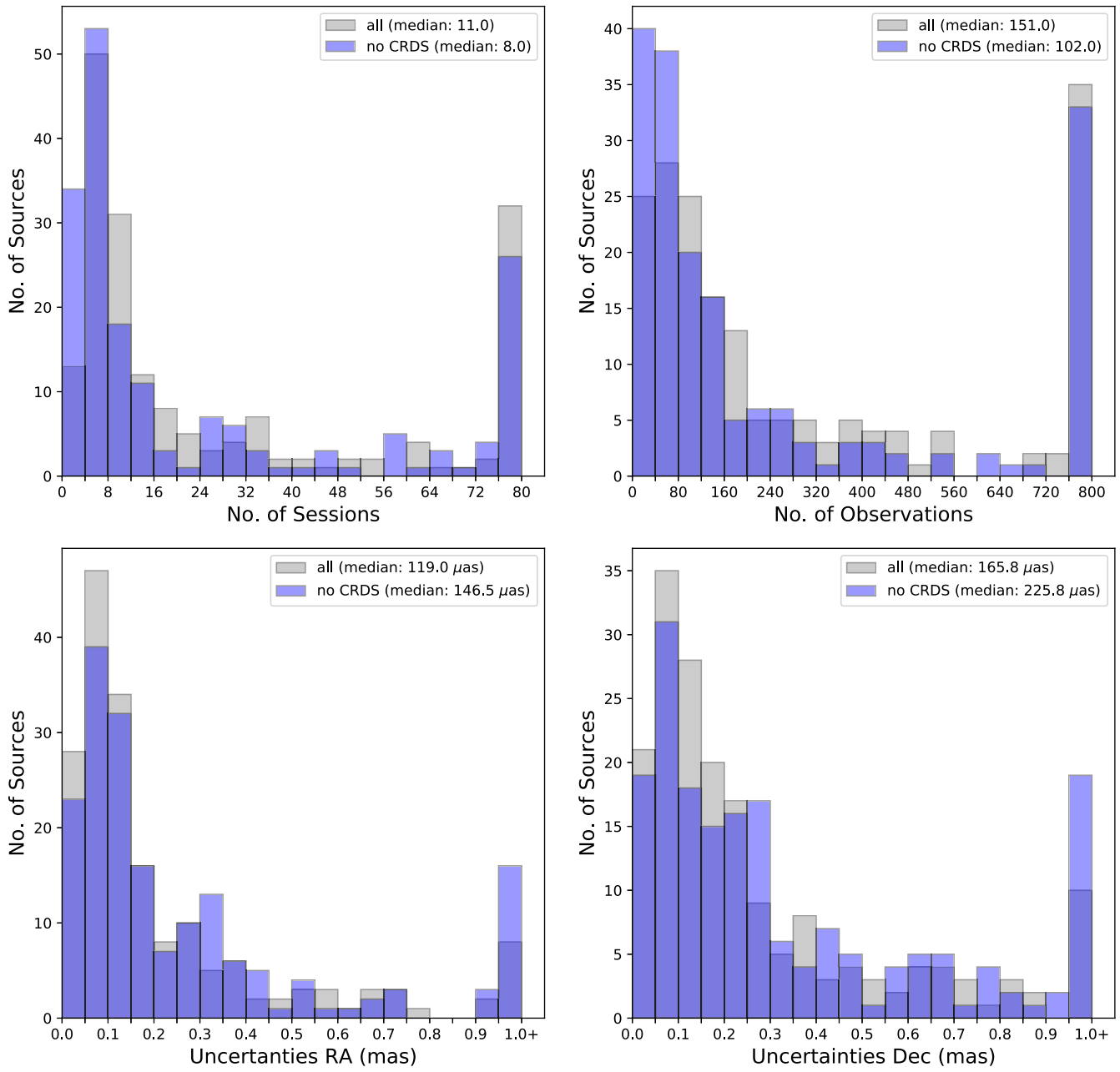

Figure 11. Comparison of statistics between a CRF solution of the 182 deep-South sources observed in CRDS sessions with all sessions (in grey) and one without the CRDS sessions between 2018 and 2021 (in blue). Median values for each distribution are listed in parenthesis.

available. An automated pipeline was used for self-calibration and imaging using the Caltech Difference Mapping software (difmap, Shepherd 1997).

A total of 185 sources were imaged from twelve CRDS sessions between 2013–2019 at both *S*- and *X*-band, with some sources imaged at multiple epochs. Table 2 lists the participating stations and the number of sources observed and imaged in each of the twelve sessions. Fig. 12 shows images for a representative sample of four sources observed in CRDS sessions between 2018 and 2019. The source 0252-549 shows a bright second component in the CRDS image in Fig. 12. No images of this source are available from the Astrogeo Radio Fundamental Catalogue (RFC, Petrov 2022). Three of the sources, 0302-623, 0454-810 and 1925-610 are ICRF2 defining sources. The source 0302-623 shows bright extended emission in the CRDS image in Fig. 12 and was removed as a defining source for the ICRF3. There are no images of this source available in the Astrogeo RFC. The source 0454-810 is an ICRF3 defining source. The CRDS image in Fig. 12 as well as images available from the Astrogeo RFC, all show a very compact structure for 0454-810. The source 1925-610 is an ICRF3 defining source and only one image, from 2010, is available from the Astrogeo RFC. The CRDS image in Fig. 12 shows a bright second component and the status of 1925-610 as an ICRF3 defining source should be revisited in future.

https://doi.org/10.1017/pasa.2023.33 Published online by Cambridge University Press

Table 2. The twelve CRDS sessions for which images have been produced.

Session name	Date yyyy-mm-dd	Participating stations	Sources observed	Sources imaged
CRDS63	2013-01-14	Hh-Ho-Ke-Yg	38	34
CRDS66	2013-07-30	Hb-Hh-Ho-Ke-Ww	38	13
CRDS68	2013-11-27	Hb-Hh-Ho-Ke-Ww-Yg	38	37
CRDS94	2018-03-21	Hh-Ht-Ke-Ww-Yg	51	26
CRDS95	2018-05-07	Hh-Ho-Ke-Ww-Yg	39	38
CRDS96	2018-06-20	Hh-Ho-Ke-Ww-Yg	44	43
CRDS97	2018-08-14	Hh-Ho-Ke-Ww-Yg	52	52
CRDS98	2018-09-26	Hh-Ho-Ke-Ww-Yg	54	51
CRD100	2019-02-18	Hh-Ho-Ke-Ww-Yg	50	50
CRD101	2019-03-27	Hh-Ke-Ww-Yg	53	45
CRD102	2019-05-06	Hh-Ho-Ke-Oh-Ww-Yg	36	36
CRD103	2019-06-25	Hh-Ho-Oh-Ww-Yg	37	37

4.3. Performance

The performance of VLBI relies on a global network of antennas, owned and operated by many diverse organisations. The loss of any one antenna can have a huge knock-on effect by removing multiple baselines, which has a compounded impact on the observations available for analysis. It is important to note that for an array of N antennas there will be $N(N-1)/2$ baselines. Thus for example taking an array of 5 antennas gives 10 baselines, losing one antenna reduces the number of baselines to 6; a 40% reduction. An antenna or multiples can be lost due to mechanical, electrical, or other issues for a whole or part of a 24-h session.

Even though scans within observations can be correlated, poor performance by one antenna for many reasons will also impact those actually used in the analysis. For example, scheduling an antenna with the wrong system equivalent flux density (SEFD) ora physical issue such as a cooled receiver having a fault and running hot/warm. A warm receiver will greatly reduce the sensitivity of an antenna. The resulting performance will be in some sense equivalent to the station having a cold receiver but observing for (typically) only one-third of the nominal time and therefore recording the equivalent of only one-third of the expected bits. Also, poor pointing can be converted into an equivalent lost sensitivity and then equivalent fraction of lost bits. RFI is becoming much more prevalent and an issue for many stations at *S*-Band (2–3 GHz), which also causes scans to be excluded by the correlator and be unavailable for the analysis. The per session statistics from the analysis reports ordered by session number are shown in Fig. 13 and show the result of some of the above issues (A compilation of the CRDS53-116 session statistics are presented in 7). In the figure and the appendix scheduled/correlated/recoverable/used observations are defined thus. Within a 24 h IVS session multiple observations of sources with different baselines and stations are schedule, these observations are defined as **scheduled**. Of these observations not all are able to be correlated for various reasons, so the number able to be correlated is less than the number scheduled and is presented here as **Correlated.** Even though a scheduled observation is able to be correlated it might not be usable for analysis, so we have the number **Recoverable**. Then number **Used** are those able to be actually applied for the final analysis and data solution.

One of the open problems, evident from the session statistics, is that only a small percentage of the observations from the CRDS sessions are actually used for analysis (on average ≈44%). However, closer inspection of the analysis reports shows that the main contributor to this high failure rate is the long baseline observations by the smaller antennas. The Ag and Oh antennas are both small dishes with large SEFDs (>10000 Jy) and are mostly tagged-along in the CRDS schedules. Stations that are scheduled in tagged-along mode are not essential as scheduled for the analysis, but can provide additional data that might be useful. This is common practice for new stations or after a major station upgrade or change until the data quality has been assessed and is acceptable to become a fully participating network station. In Fig. 14 the actual number of scans scheduled by baseline is shown. In Fig. 15 there are the % of scheduled versus used by baseline.

The post-fit residual delay rms values over all observations of the CRDS schedules are presented in Fig. 16. We find a median session fit of 37 ps over all the CRDS sessions we have data for; this is comparable with the IVS R1/R4 observations with a median value of 34 ps (Plank et al. 2017).

5. Discussion and future plans

The primary purpose of the CRDS programme is to improve the CRF in the Southern Hemisphere. Since 2018 January, various improvements were made to CRDS sessions, e.g., the data rate was increased from 256 Mbps to 1 Gbps, the frequency sequence was optimised to avoid RFI, the scheduling was improved and optimised for both astrometry and imaging, and the source list was expanded. In addition, in 2021, three large antennas Km, Sc, and Mk, were added to the CRDS sessions to increase the number of stations and sensitivity of the existing network. However, the addition of these northern stations will only improve the results for sources down to about −50° Dec and not for sources in the Deep-South. Initially there were scheduling issues for Sc and Mk as the hardware setup was incorrect in the distributed VEX file, causing these stations to be unable to participate in CRD114, 115, and 116. Furthermore, scheduling of these CRDS sessions which include Northern antennas is problematic. In addition, the transitioning of the Australian 12-m telescopes to VGOS broad-band and the temporary removal of the Hobart 26-m telescope in Australia and then the Warkworth 12-m in New Zealand due to repairs, has had a major impact on the CRDS sessions and the CRF in the Deep-South.

For future CRDS observations into the next decade, we hope to increase the data of the CRDS sessions, further improving the sensitivity. For existing stations an increase in the data recording rate from 1 to 2 Gbps is possible. An improvement in sensitivity can be used in two possible ways, one to observe sources for a shorter period and allowing for an increase in the number of sources and/or observations per session; second to add further weaker sources that will improve the coverage and density of sources in the Southern Hemisphere.

We anticipate the repair and return of the Ho and Ww antennas in the near future, and potentially adding additional southern stations to the CRDS network, such as the antennas forming part of the Long Baseline Array (LBA). However, most of the LBA antennas are not currently capable of dual-band *S*/*X* observations.

https://doi.org/10.1017/pasa.2023.33 Published online by Cambridge University Press

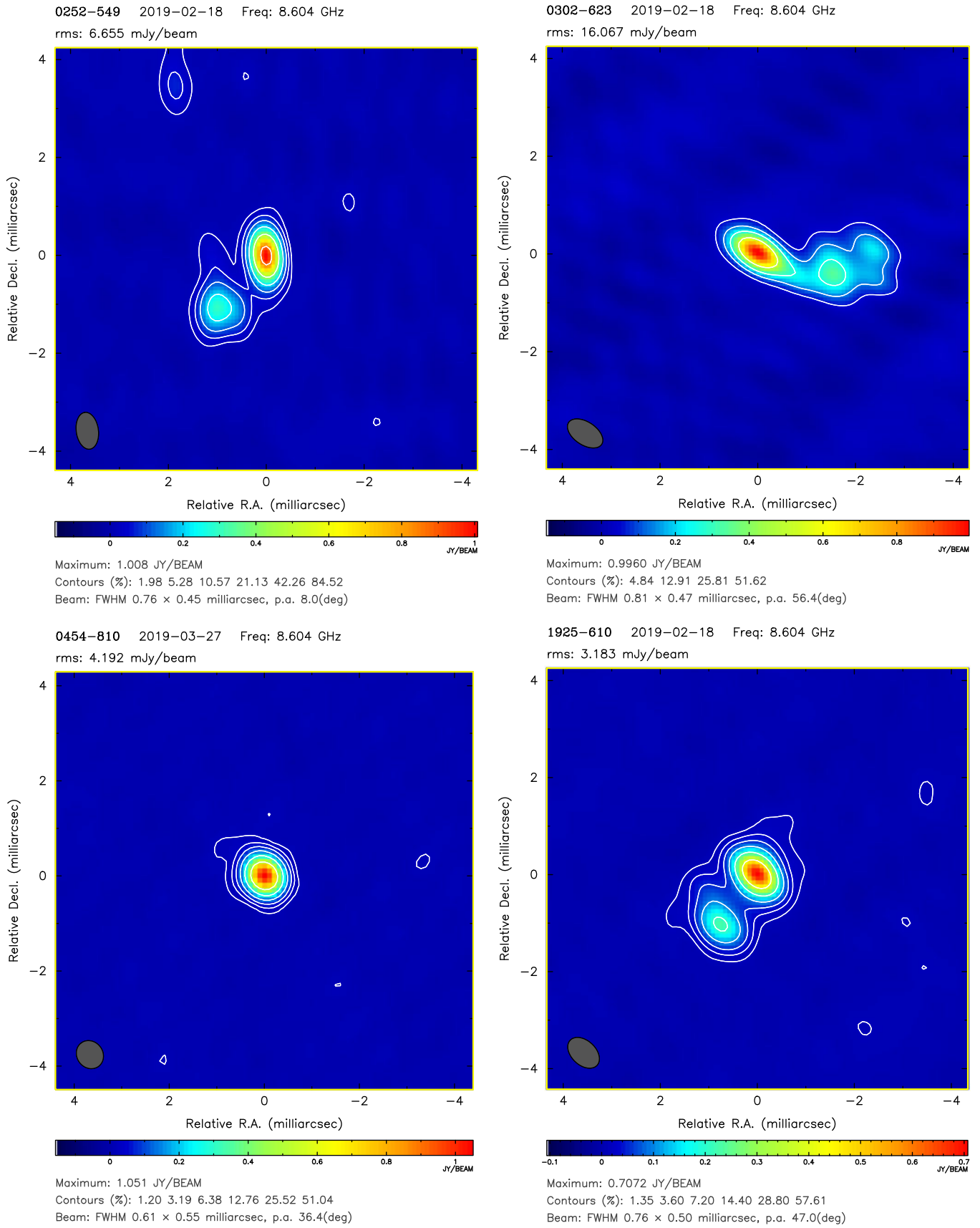

Figure 12. Colour maps with contours for sources 0252-549 (top left), 0302-623 (top right), 0454-810 (bottom left), and 1925-610 (bottom right) at 8.6 GHz from CRDS sessions between 2018 and 2019. North is Up and East is to the Left. The Full Width Half Maximum (FWHM) beam size is graphically indicated in the bottom left corner.

https://doi.org/10.1017/pasa.2023.33 Published online by Cambridge University Press

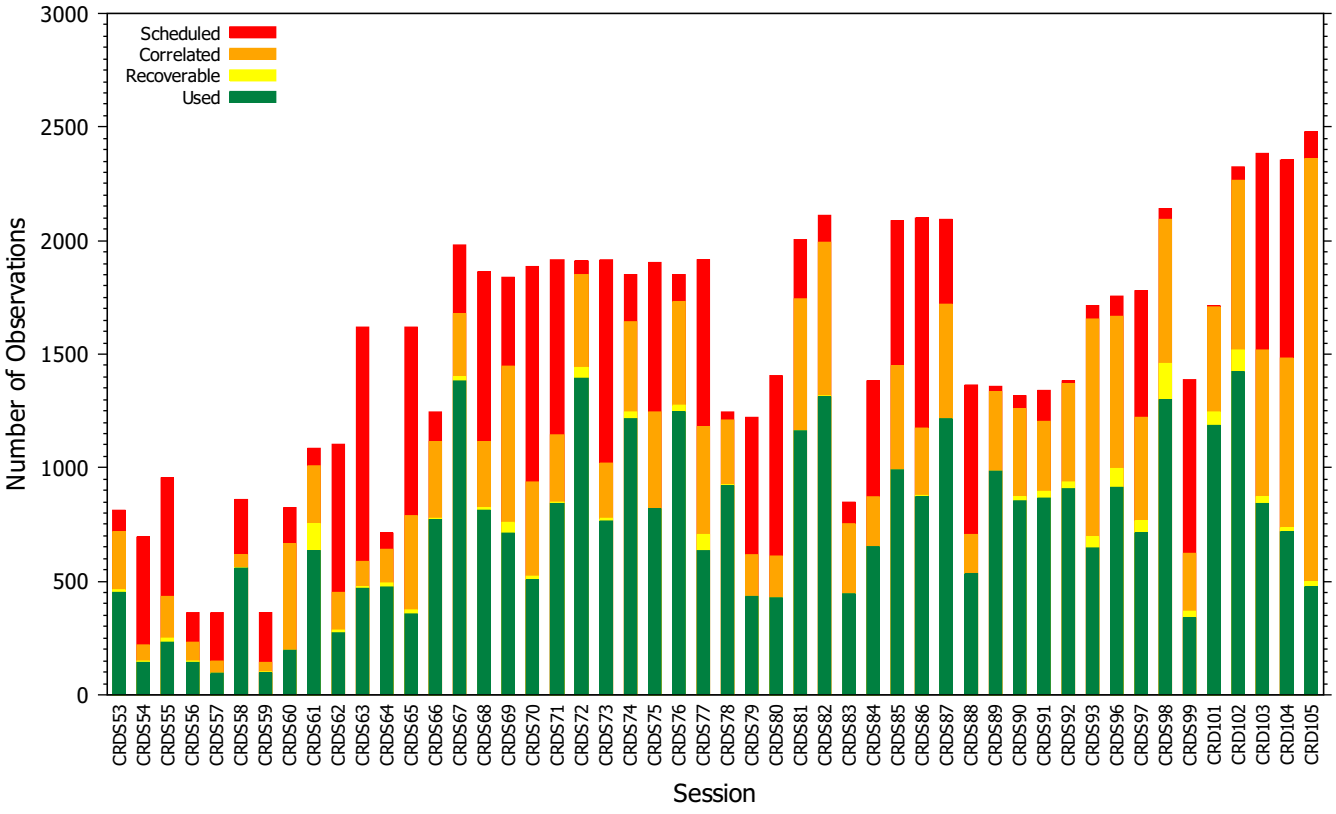

Figure 13. The per session statistics from the analysis reports ordered by time. In red is the total number of observations per session scheduled; in orange are those that were able to be correlated; in yellow is the number able to be recovered for analysis and in green are the number of observations used in the analysis solution.

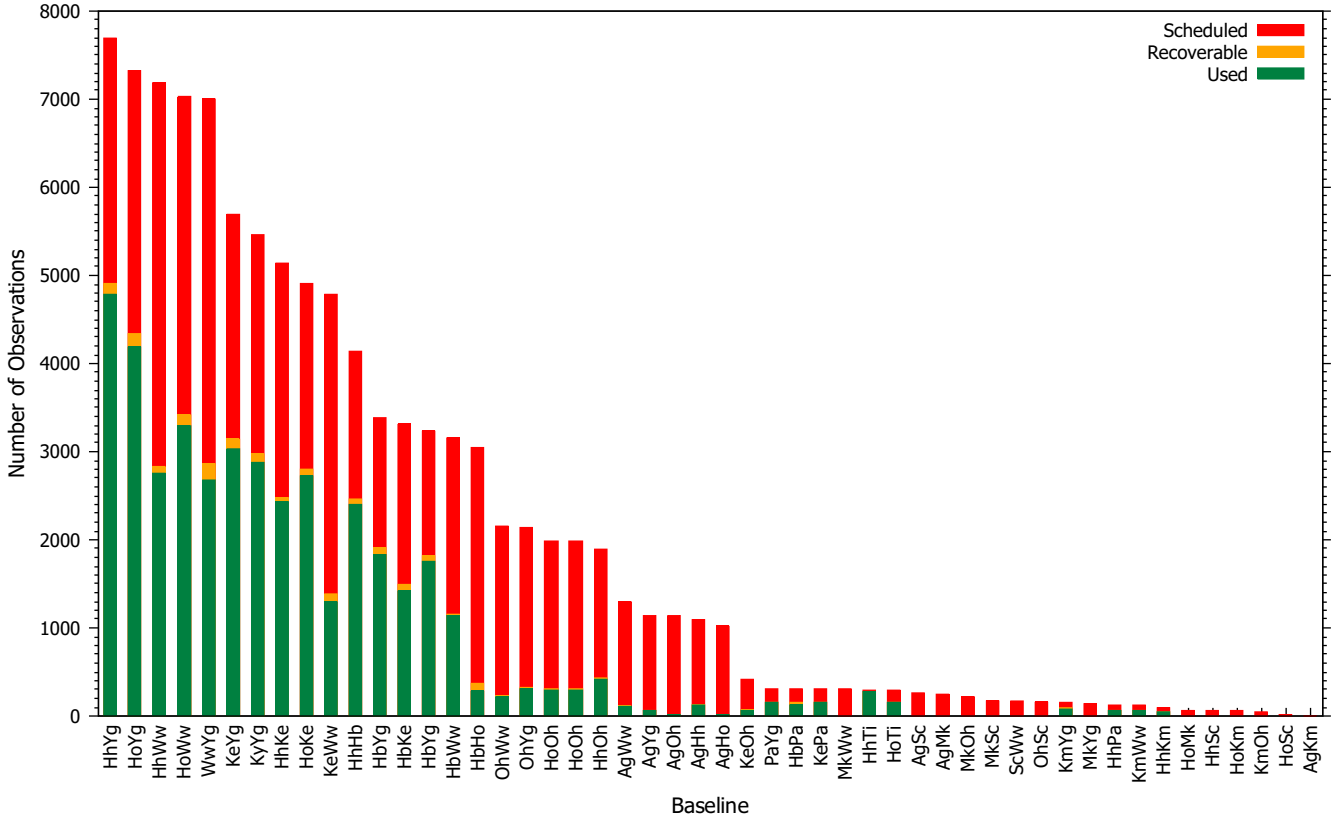

Figure 14. The number of observations made by each baseline from the analysis reports, ordered by the number of scheduled observations greatest to lowest from right to left. In red is the total number of observations scheduled; orange are those that were able to be recovered; and green are the number of observations used in the analysis solution.

https://doi.org/10.1017/pasa.2023.33 Published online by Cambridge University Press

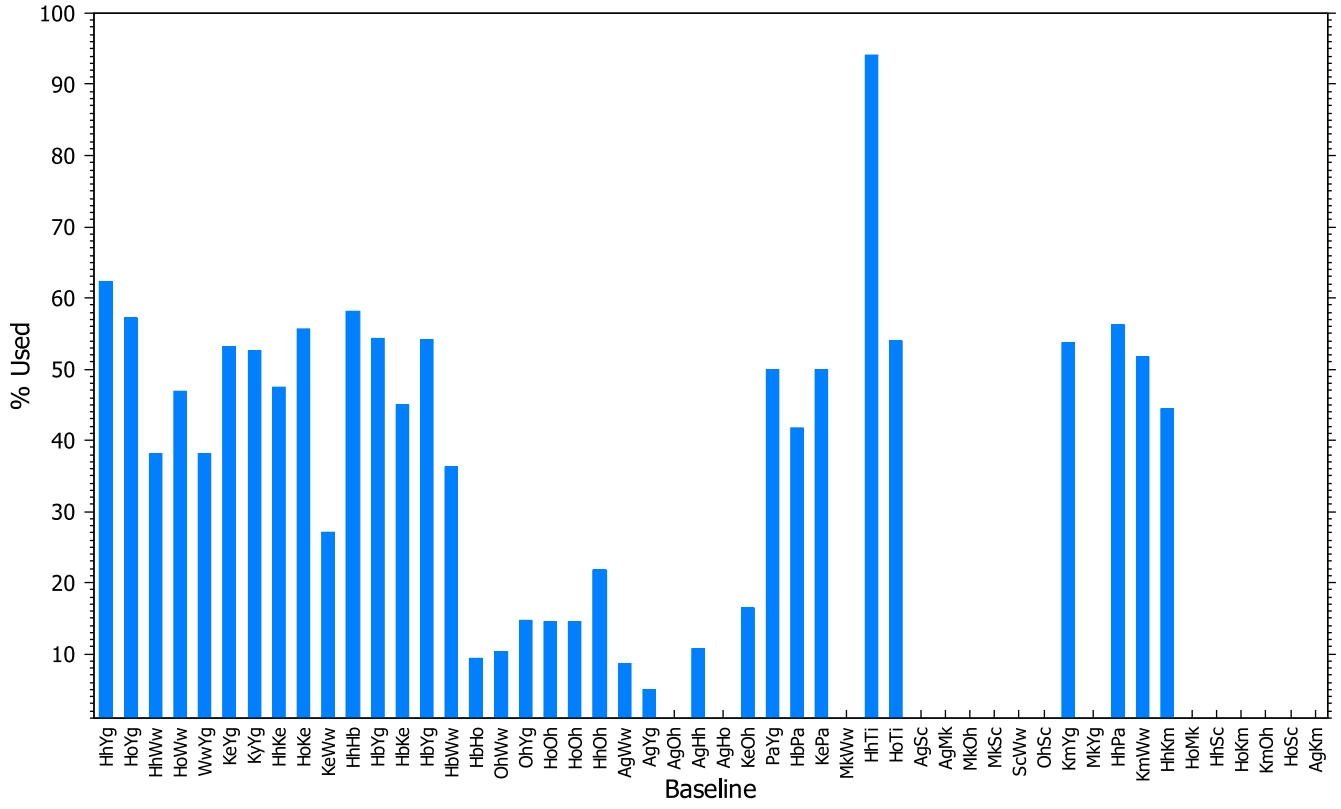

Figure 15. This figure shows the percentage of observations out of those scheduled which were used in an analysis solution by baseline. The order of the baselines is the same as in Fig. 14 to aid comparing the two figures.

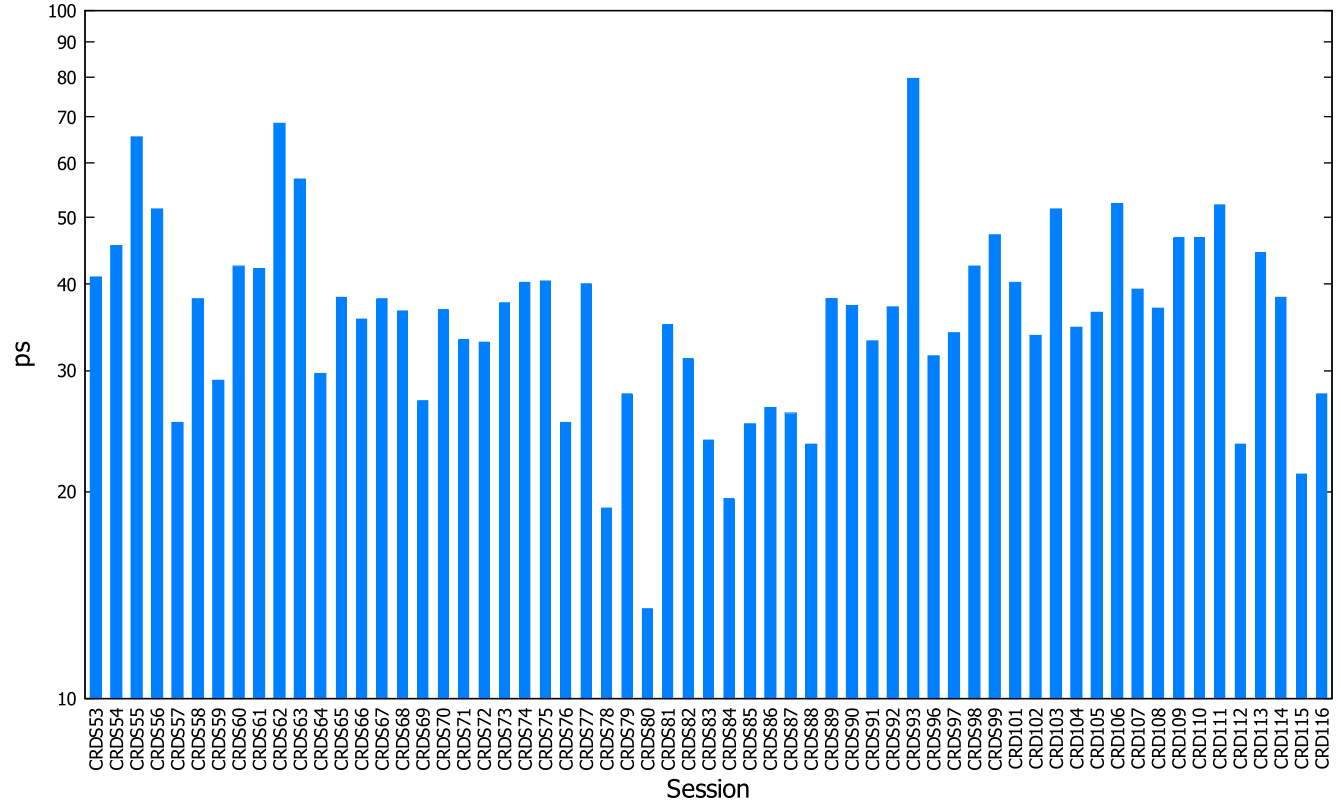

Figure 16. The post-fit residual delay rms values over all observations of a CRDS schedule, ordered by session reference code.

https://doi.org/10.1017/pasa.2023.33 Published online by Cambridge University Press

Another possibility is adding one of the Tidbinbilla antennas in Australia to the CRDS network. However, the Tidbinbilla antennas are only available for a few hours per 24-h session. The 34-m Tidbinbilla antennas may be available for longer, while time on the 70-m antenna is difficult to get and the slew rates are slow (0.25 deg s^{-1}). On the other hand, the Hb and Ke 12-m VGOS antennas are available for use in mixed-mode observations, and correlation of mixed-mode CRDS sessions needs to be investigated further.

We have also investigated the possibility of adding large sensitive antennas operating in single band (X) mode only, e.g., the 30 m Warkworth antenna in New Zealand. However, the possible shutdown of the Warkworth observatory may result in the loss of both the 12-m and 30-m Warkworth antennas. We are also investigating the possibility of including larger more sensitive stations in South America, The Zapala station is equipped with a 35-m antenna but there are no plans to install a wider *S*/*X* band receiver in the near future. There is also a plan to built a 40-m general purpose radio telescope in San Juan (China-Argentina Radio Telescope, CART). As of 2020, the antenna foundation has been completed, but the antenna delivery and installation was postponed due to the COVID-19 pandemic. This antenna, once completed, could be a promising candidate for CRF work.

It is expected that with the addition of new stations, better knowledge of sources such as flux density and source structure from imaging should lead to improved scheduling. As a result of these and other steps, further improvements to the ICRF will be obtained for the Southern Hemisphere in the years ahead.

Acknowledgement. We wish to acknowledge the International VLBI Service for Geodesy & Astrometry (IVS) for providing the organisational infrastructure that was essential to this work. In addition we would like to recognise the many organisations that under the IVS umbrella provide the Network Stations, Operation Centres, Correlators, Data Centres, Analysts Centres and the Technology Development Centres.

The research was carried out in part at the Jet Propulsion Laboratory, California Institute of Technology, under a contract with the National Aeronautics and Space Administration (80NM0018D0004).

From the 2023 July 1 operation of Warkworth will be transferred from AUT University to Space Operations New Zealand Ltd with new funding from Land Information New Zealand (LINZ).

Data Availability Statement. The final data products from this work are stored in three primary IVS Data Centers hosted at the Paris Observatory Data Center, OPAR (Barache et al. 2021); the Federal Agency for Cartography and Geodesy, Germany Data Center, BKG (Girdiuk et al. 2021); and the GSFC's Crustal Dynamics Data Information System, CDDIS (Michael and Blevins 2021).

The three primary IVS Data Centres mirror each other several times during the day to ensure common consistent holdings. Access is free for users and data can be accessed from the url's provided in the following list:

OPAR using FTP at ftp://ivsopar.obspm.fr

BKG using FTP at ftp://ivs.bkg.bund.de/pub/vlbi and HTTP at https://ivs.bkg.bund.de/data_dir/vlbi/

GSFC via the Crustal Dynamics Data Information System (CDDIS) at https://cddis.nasa.gov/archive/vlbi/

How to access the data and products is different for each data centre, and users will have to familiarise themselves with the methods and processes to extract the required data.

References

Alef, W., & Graham, D. A. 2002, in Proceedings of the 6th EVN Symposium

Altamimi, Z., Rebischung, P., Collilieux, X., Metivier, L., & Chanard, K. 2022, in EGU General Assembly Conference Abstracts, EGU22–3958

Altamimi, Z., Rebischung, P., Metivier, L., Collilieux, X., Chanard, K., & Teyssendier-de-la-Serve, M. 2021, in EGU General Assembly 2021, https://doi.org/ 10.5194/egusphere-egu21-2056

Bachmann, S., Hellmers, H., Schneider-Lock, S., Geist, S., Thaller, D., Bloßfeld, M., & Seitz, M. 2021, in International VLBI Service for Geodesy and Astrometry 2019+2020 Biennial Report, ed. D. Behrend, K. D. Baver, & K. L. Armstrong

Barache, C., Carlucci, T., Becker, O. & Lambert, S. 2021, in International VLBI Service for Geodesy and Astrometry 2019+2020 Biennial Report, ed. D. Behrend, K. L. Armstrong, & K. D. Baver

Basu, S., de Witt, A. & Gattano, C. 2021, in Proceedings of the 25th Working Meeting of the European VLBI Group for Geodesy, ed. R. Haas, P7

Basu, S., de Witt, A., Quick, J., & Malkin, Z. 2018, in 14th European VLBI Network Symposium & Users Meeting (EVN 2018), 135

Basu, S., de Witt, A., Shabala, S., McCallum, J., Quick, J. & Bertarini, A. 2016, in New Horizons with VGOS, ed. D. Behrend, K. D. Baver, & K. L. Armstrong, 312

Beasley, A. J., & Conway, J. E. 1995, in Astronomical Society of the Pacific Conference Series, 82, 327

Behrend, D. 2018, 39th IVS Directing Board Meeting

Behrend, D. 2019, 41st IVS Directing Board Meeting

Behrend, D. 2020, 42nd IVS Directing Board Meeting

Bolotin, S., Baver, K., Gipson, J., Gordon, D. & MacMillan, D. 2014, in International VLBI Service for Geodesy and Astrometry 2014 General Meeting Proceedings: "VGOS: the New VLBI Network, 253

Carter, E. W., & Robertson, D. S. 1993, in Developments in Astrometry and their Impact on Astrophysics and Geodynamics, 156, 133, https://doi.org/10.1007/978-94-011-1711-127

Charlot, P. 1990, AJ 99, 1309, https://doi.org/10.1086/115419

Charlot, P. 2018, in 14th European VLBI Network Symposium & Users Meeting (EVN 2018), 136

Charlot, P., et al. 2020, A&A, 644, A159, https://doi.org/10.1051/0004-6361/202038368. arXiv: 2010.13625 [astro-ph.GA].

de Witt, A., et al. 2021, in 25th European VLBI Group for Geodesy and Astrometry Working Meeting, ed. R. Haas, 25, 85

de Witt, A., Le Bail, K., Jacobs, C., Gordon, D., Mayer, D., Schartner, M., & Basu, S. 2019, in International VLBI Service for Geodesy and Astrometry 2018 General Meeting Proceedings: "Global Geodesy and the Role of VGOS - Fundamental to Sustainable Development, 189

de Witt, A., et al. 2019, in 24th Meeting of the European VLBI Group for Geodesy and Astrometry (EVGA)

de Witt, P., Charlot, A., Jacobs, C. S. & Gordon, D. 2022, MDPI (Universe) 8, IssN: 2218-1997, https://www.mdpi.com/2218-1997/8/7/374

Deller, A. T., et al. 2011, 123, 275, https://doi.org/10.1086/658907. arXiv: 1101.0885 [astro-ph.IM].

Eubanks, T. M. 1993, in Contributions of Space Geodesy to Geodynamics: Earth Dynamics, 24, 1, https://doi.org/10.1029/GD024p0001

Fey, A., Ojha, R., Boboltz, D., Geiger, N., Kingham, K., Hall, D., Gaume, R. & Johnston, K. 2010, in Sixth International VLBI Service for Geodesy and Astronomy. Proceedings from the 2010 General Meeting, ed. R. Navarro, S. Rogstad, C. E. Goodhart, E. Sigman, M. Soriano, D. Wang, Leslie A. WHITE, & C. S. Jacobs, 153

Fey, A. L., et al. 2015, AJ, 150, 58, https://doi.org/10.1088/0004-6256/150/2/58

Fomalont, E., Kopeikin, S., Lanyi, G., & Benson, J. 2009, ApJ, 699, 1395, https://doi.org/10.1088/0004-637X/699/2/1395. arXiv: 0904.3992[astro-ph.CO].

Fricke, W., et al. 1988, VeARI 32, 1

Gattano, C., Lambert, S. B. & Le Bail, K. 2018, A&A, 618, A80, https://doi.org/10.1051/0004-6361/201833430

Girdiuk, A., Goltz, M., Engelhardt, G., & Ullrich, D. 2021, in International VLBI Service for Geodesy and Astrometry 2019+2020 Biennial Report, ed. D. Behrend, K. D. Baver, & K. L. Armstrong

Gordon, D., de Witt, A. & Jacobs, C. S. 2022, in 12th IVS General Meeting, Helsinki, Finland (Virtual)
Greisen, E. W. 2003, in Information Handling in Astronomy - Historical Vistas, ed. A. Heck (Dordrecht: Kluwer Academic Publishers), 285, 109. https://doi.org/10.1007/0-306- 48080-8_7
Gulyaev, S., & Natusch, T. 2010, in International VLBI Service for Geodesy and Astrometry 2009 Annual Report, ed. D. Behrend, & K. D. Baver
Hall, D. M., & Veillette, D. 2015, in International VLBI Service for Geodesy and Astrometry 2014 Annual Report, ed. D. Behrend, K. D. Baver, & K. L. Armstrong
Heinkelmann, R., et al. 2011, JG, 85, 377, https://doi.org/10.1007/s00190-011-0459-x
Hellmers, H., Bachmann, S., Thaller, D., Bloßfeld, M. & Seitz, M. 2021, in Egu General Assembly Conference Abstracts, EGU21–10678. EGU General Assembly Conference Abstracts, https://doi.org/10.5194/egusphe re-egu21-10678
Hungwe, F., Ojha, R., Booth, R. S., Bietenholz, M. F., Collioud, A., Charlot, P., Boboltz, D. & Fey, A. L. 2011, MNRAS, 418, 2113, https://doi.org/10.1111/j.1365-2966.2011.19232.x. arXiv: 1106.2669 [astro-ph.CO].
IVS. 2021, IVS Analysis, https://ivscc.gsfc.nasa.gov/analysis/index.html
Lovell, J. E., et al. 2013. JG, 87, 527, https://doi.org/10.1007/s00190-013-0626-3. arXiv: 1304.3213 [astro-ph.IM].
Ma, C., et al. 1998, AJ, 116, 516, https://doi.org/10. 1086/300408
Ma, C. 1978, PhD diss., University of Maryland, College Park
MacMillan, D. S., et al. 2019, A&A, 630, A93, https://doi.org/10.1051/0004-6361/201935379
McCallum, L., Wakasugi, T. & Shu, F. 2019, in International VLBI Service for Geodesy and Astrometry 2018 General Meeting Proceedings: "Global Geodesy and the Role of VGOS - Fundamental to Sustainable Development, 131
Michael, P., & Blevins, S. 2021, Technical report. NASA-TP-20210021389
MIT Haystack Observatory. 2021, https://www.haystack.mit.edu/haystack-observatory-postprocessing-system-hops/
Nothnagel, A., Artz, T., Behrend, D., & Malkin, Z. 2017, JG, 91, 711, https://doi.org/10.1007/s00190-016-0950-5
Park, R. S., Folkner, W. M., Williams, J. G. & Boggs, D. H. 2021, AJ, 161, 105, https://doi.org/10. 3847/1538-3881/abd414
Petrachenko, W., Behrend, D., Hase, H., Ma, C., Niell, A., Schuh, H., & Whitney, A. 2013, in EGU General Assembly Conference Abstracts, EGU2013– 12867. EGU General Assembly Conference Abstracts
Petrov, L. 2022, Radio fundamental catalog. astro-geo center
Petrov, L., de Witt, A., Sadler, E. M., Phillips, C., & Horiuchi, S. 2019, MNRAS, 485, 88, https://doi.org/10.1093/mnras/stz242. arXiv: 1812.02916 [astro-ph.IM]
Plank, L., et al. 2017, JG, 91, 803, https://doi.org/10.1007/s00190-016-0949-y
Rioja, M. J., & Dodson, R. 2020, A&A, 28, 6, https://doi.org/10.1007/s00159-020-00126-z. arXiv: 2010.02156 [astro-ph.IM].
Schartner, M., & Böhm, J. 2019, PASP, 131, 084501, https://doi.org/10.1088/1538-3873/ab1820
Shepherd, M. C. 1997, in Astronomical Data Analysis Software and Systems VI, Astronomical Society of the Pacific Conference Series, ed. G. Hunt, & H. Payne, 125, 77, https://ui.adsabs.harvard.edu/abs/1997ASP C.125. . .77S
Shu, F., Zheng, W., He, X., Huang, Y., Chen, Z., Zhang, J., & Kondo, T. 2018, Shanghai VLBI Correlator 2017–2018 Biennial Report
Thornton, C. L., & Border, J. S. 2000, in Deep–Space Communications and Navigation Series, Monograph 1, JPL publication 00-11, Jet Propulsion Laboratory, California Institute of Technology
Vandenberg, N. R. 1997, NVI, Inc. NASA/Goddard Space Flight Center
Walker, R. 2018, http://www.aoc.nrao.edu/software/sched/index.html
Xu, M. H., Anderson, J. M., Heinkelmann, R., Lunz, S., Schuh, H., & Wang, G. L. 2019, ApJS, 242, 5, https://doi.org/10.3847/1538-4365/ab16ea

Appendix 1. Source list for sessions CRDS50-116

This appendix contains a list of the 298 sources detected in the CRDS sessions between 2011 January and 2021 December (CRDS50–116). The format: column 1 is the IVS source name, columns 2 and 3 are the RA and declination coordinates (J2000), column 4 is the number of CRDS sessions that a source was scheduled in, and column 5 is the total number of observations of that source in all the scheduled sessions. ICRF3 defining sources are highlighted in boldface.

IVS name	RA (h) (min) (s)	Dec (°) (') (")	N_{sess}	N_{obs}
0008-300	0 10 45.18	−29 45 13.18	1	2
0010-401	0 12 59.91	−39 54 26.06	2	86
0034-220	0 37 14.83	−21 45 24.71	1	5
0035-252	**0 38 14.74**	**−24 59 2.24**	**2**	**16**
0037-593	0 40 7.85	−59 3 52.76	3	34
0048-427	0 51 9.50	−42 26 33.29	23	353
0100-760	1 2 18.66	−75 46 51.73	3	55
0104-275	1 6 26.08	−27 18 11.83	1	26
0104-408	**1 6 45.11**	**−40 34 19.96**	**28**	**649**
0107-610	**1 9 15.48**	**−60 49 48.46**	**30**	**355**
0110-668	1 12 18.91	−66 34 45.19	3	51
0113-283	1 15 23.88	−28 4 55.22	1	46
0116-219	1 18 57.26	−21 41 30.14	1	11
0122-514	1 24 57.39	−51 13 16.17	3	27
0131-522	1 33 5.76	−52 0 3.95	20	405
0142-278	1 45 3.39	−27 33 34.33	2	48
0155-549	1 56 49.71	−54 39 48.50	1	10
0159-668	2 1 7.74	−66 38 12.67	2	35
0202-765	2 2 13.69	−76 20 3.06	1	3
0206-625	2 8 1.17	−62 16 35.53	1	13
0206-689	2 7 50.93	−68 37 55.16	4	25
0208-512	**2 10 46.20**	**−51 1 1.89**	**8**	**237**
0214-522	2 16 3.20	−52 0 12.48	1	1
0219-637	2 20 54.17	−63 30 19.39	1	14
0227-369	**2 29 28.45**	**−36 43 56.82**	**1**	**2**
0227-542	2 29 12.79	−54 3 24.03	1	7
0229-479	2 31 11.80	−47 46 11.58	3	95
0230-790	**2 29 34.95**	**−78 47 45.60**	**30**	**751**
0234-301	**2 36 31.17**	**−29 53 55.54**	**2**	**24**
0235-618	**2 36 53.25**	**−61 36 15.18**	**21**	**159**
0241-564	2 43 26.53	−56 12 42.44	1	1
0252-549	2 53 29.18	−54 41 51.44	5	179
0302-623	3 3 50.63	−62 11 25.55	29	667
0308-611	**3 9 56.10**	**−60 58 39.06**	**27**	**727**
0312-770	3 11 55.25	−76 51 50.85	7	194
0332-403	**3 34 13.65**	**−40 8 25.40**	**27**	**643**
0334-546	3 35 53.92	−54 30 25.11	24	486
0346-279	**3 48 38.14**	**−27 49 13.57**	**3**	**33**
0347-211	**3 49 57.83**	**−21 2 47.74**	**1**	**16**
0355-483	3 57 21.92	−48 12 15.16	1	17
0355-669	**3 55 47.88**	**−66 45 33.82**	**6**	**71**

https://doi.org/10.1017/pasa.2023.33 Published online by Cambridge University Press

0400-319	**4 2 21.27**	**−31 47 25.95**	**3**	**64**
0402-362	**4 3 53.75**	**−36 5 1.91**	**24**	**480**
0405-385	4 6 59.04	−38 26 28.04	21	542
0431-512	4 32 21.18	−51 9 25.19	1	5
0432-606	4 33 34.11	−60 30 13.77	2	29
0437-454	**4 39 0.85**	**−45 22 22.56**	**23**	**574**
0440-520	4 41 58.28	−51 54 54.17	1	13
0441-699	4 40 47.76	−69 52 18.09	2	72
0450-743	4 48 48.56	−74 17 31.25	1	25
0454-234	**4 57 3.18**	**−23 24 52.02**	**4**	**63**
0454-810	**4 50 5.44**	**−81 1 2.23**	**35**	**1064**
0506-612	**5 6 43.99**	**−61 9 40.99**	**25**	**419**
0507-611	5 7 54.67	−61 4 43.12	1	15
0514-459	5 15 45.25	−45 56 43.20	1	12
0516-621	5 16 44.93	−62 7 5.39	27	776
0517-726	5 16 37.72	−72 37 7.47	1	40
0521-262	5 23 18.47	−26 14 9.55	1	26
0522-611	**5 22 34.43**	**−61 7 57.13**	**24**	**303**
0523-236	5 25 6.51	−23 38 10.81	1	44
0524-460	5 25 31.40	−45 57 54.69	13	48
0524-485	**5 26 16.67**	**−48 30 36.79**	**29**	**472**
0530-727	**5 29 30.04**	**−72 45 28.51**	**5**	**193**
0534-340	**5 36 28.43**	**−34 1 11.47**	**23**	**478**
0534-611	5 34 35.77	−61 6 7.07	20	535
0537-286	**5 39 54.28**	**−28 39 55.95**	**4**	**75**
0537-441	5 38 50.36	−44 5 8.94	21	507
0542-735	5 41 50.78	−73 32 15.35	4	71
0549-575	5 50 9.58	−57 32 24.40	26	567
0601-706	6 1 11.25	−70 36 8.79	3	77
0610-436	6 12 28.61	−43 37 48.38	1	8
0621-787	6 18 30.16	−78 43 2.14	5	170
0622-441	6 23 31.79	−44 13 2.55	1	6
0622-645	6 23 7.70	−64 36 20.72	1	6
0624-546	6 25 52.23	−54 38 50.71	1	22
0627-199	**6 29 23.76**	**−19 59 19.72**	**2**	**12**
0628-627	6 28 57.49	−62 48 44.74	1	33
0628-671	6 28 39.61	−67 12 47.41	1	8
0634-584	6 35 40.83	−58 27 10.28	1	4
0642-349	**6 44 25.28**	**−34 59 41.95**	**1**	**6**
0646-306	**6 48 14.10**	**−30 44 19.66**	**4**	**69**
0700-197	**7 2 42.90**	**−19 51 22.04**	**1**	**8**
0700-465	**7 1 34.55**	**−46 34 36.63**	**3**	**6**
0738-674	**7 38 56.50**	**−67 35 50.83**	**5**	**61**
0742-562	**7 43 20.49**	**−56 19 32.96**	**5**	**84**
0743-673	7 43 31.61	−67 26 25.55	1	24
0744-691	7 44 20.39	−69 19 7.16	1	18
0804-267	**8 6 12.72**	**−26 52 33.31**	**5**	**25**
0809-493	**8 11 8.80**	**−49 29 43.51**	**1**	**2**
0820-578	8 21 20.53	−58 0 18.75	1	6
0823-500	8 25 26.87	−50 10 38.49	1	3
0826-373	**8 28 4.78**	**−37 31 6.28**	**4**	**105**
0834-201	**8 36 39.22**	**−20 16 59.50**	**6**	**52**
0842-754	8 41 27.04	−75 40 27.87	1	8
0843-547	8 45 2.48	−54 58 8.54	4	47
0848-588	8 49 14.88	−59 5 0.77	1	4
0851-577	8 52 38.73	−57 55 29.81	2	98
0855-716	**8 55 11.77**	**−71 49 6.46**	**3**	**35**
0858-279	9 0 40.04	−28 8 20.34	1	11
0903-573	9 4 53.18	−57 35 5.78	4	138
0918-534	**9 19 44.04**	**−53 40 6.45**	**4**	**22**
0920-397	9 22 46.42	−39 59 35.07	23	584
0936-853	9 30 32.57	−85 33 59.70	4	54
0944-469	9 46 51.34	−47 7 59.23	2	26
0956-409	9 58 38.30	−41 10 33.17	1	19
0959-443	10 1 59.91	−44 38 0.60	1	8
1004-217	**10 6 46.41**	**−21 59 20.41**	**1**	**4**
1004-500	**10 6 14.01**	**−50 18 13.47**	**23**	**534**
1005-739	10 6 4.15	−74 9 44.09	1	29
1012-448	10 14 50.35	−45 8 41.15	7	117
1016-311	**10 18 28.75**	**−31 23 53.85**	**1**	**5**
1022-665	**10 23 43.53**	**−66 46 48.72**	**25**	**664**
1034-374	**10 36 53.44**	**−37 44 15.07**	**24**	**541**
1036-431	10 38 14.70	−43 25 45.89	1	14
1036-529	**10 38 40.66**	**−53 11 43.27**	**5**	**126**
1039-474	10 41 44.65	−47 40 0.07	8	253
1041-452	10 43 51.42	−45 30 9.56	1	8
1045-188	10 48 6.62	−19 9 35.73	1	12
1045-620	10 47 42.95	−62 17 14.63	5	126
1048-470	10 50 53.40	−47 19 4.55	1	9
1048-526	10 50 38.03	−52 49 48.33	2	56
1049-534	10 51 9.10	−53 44 46.54	1	51
1059-631	11 1 54.38	−63 25 22.60	4	69
1101-536	**11 3 52.22**	**−53 57 0.70**	**26**	**573**
1105-680	11 7 12.70	−68 20 50.73	2	40
1109-567	11 12 7.27	−57 3 39.75	5	56
1116-462	**11 18 26.96**	**−46 34 15.00**	**6**	**195**
1117-270	11 20 16.19	−27 19 6.37	1	40
1124-186	**11 27 4.39**	**−18 57 17.44**	**1**	**9**
1129-580	11 31 43.29	−58 18 53.44	8	216
1130-741	11 32 19.11	−74 25 9.02	1	1
1133-681	11 36 2.10	−68 27 5.82	2	80
1133-739	11 36 9.66	−74 15 45.27	2	15
1143-245	**11 46 8.10**	**−24 47 32.90**	**1**	**7**
1143-332	**11 46 28.45**	**−33 28 42.63**	**1**	**4**
1143-696	**11 45 53.62**	**−69 54 1.80**	**26**	**641**
1144-379	**11 47 1.37**	**−38 12 11.02**	**27**	**824**

https://doi.org/10.1017/pasa.2023.33 Published online by Cambridge University Press

1148-671	11 51 13.43	−67 28 11.09	4	136
1151-348	11 54 21.79	−35 5 29.06	1	11
1156-663	11 59 18.31	−66 35 39.43	22	124
1206-238	12 9 2.45	−24 6 20.76	1	17
1213-172	12 15 46.75	−17 31 45.40	1	12
1214-609	12 17 5.63	−61 13 25.43	2	4
1215-457	12 18 6.25	−46 0 28.99	5	20
1236-684	12 39 46.65	−68 45 30.89	2	8
1244-255	**12 46 46.80**	**−25 47 49.29**	**7**	**137**
1245-454	**12 48 28.50**	**−45 59 47.18**	**5**	**110**
1249-673	12 52 43.21	−67 37 38.75	1	44
1251-713	**12 54 59.92**	**−71 38 18.44**	**29**	**705**
1256-220	12 58 54.48	−22 19 31.13	2	56
1300-554	13 3 49.22	−55 40 31.61	1	23
1306-395	**13 9 48.49**	**−39 48 33.09**	**2**	**21**
1307-556	13 10 43.36	−55 52 11.53	1	9
1312-533	**13 15 4.18**	**−53 34 35.87**	**5**	**94**
1313-333	**13 16 7.99**	**−33 38 59.17**	**24**	**488**
1323-527	13 26 49.23	−52 56 23.63	3	115
1325-558	**13 29 1.14**	**−56 8 2.67**	**25**	**629**
1326-698	13 30 11.08	−70 3 13.08	3	128
1334-649	13 37 52.45	−65 9 24.90	4	25
1336-260	13 39 19.89	−26 20 30.50	1	18
1343-601	13 46 49.04	−60 24 29.36	6	12
1349-439	13 52 56.53	−44 12 40.39	20	210
1352-632	13 55 46.61	−63 26 42.57	6	14
1406-267	**14 9 50.17**	**−26 57 36.98**	**2**	**52**
1412-368	**14 15 26.02**	**−37 5 26.97**	**2**	**8**
1417-782	14 23 43.55	−78 29 34.90	5	125
1420-679	**14 24 55.56**	**−68 7 58.09**	**33**	**833**
1420-725	14 24 52.24	−72 41 17.09	6	119
1424-418	**14 27 56.30**	**−42 6 19.44**	**23**	**469**
1435-218	**14 38 9.47**	**−22 4 54.75**	**1**	**8**
1448-648	**14 52 39.68**	**−65 2 3.43**	**22**	**309**
1451-400	**14 54 32.91**	**−40 12 32.51**	**23**	**243**
1505-304	15 8 52.99	−30 36 29.43	1	11
1505-496	15 8 38.94	−49 53 2.31	5	117
1509-564	15 12 55.82	−56 40 30.64	1	1
1511-476	**15 14 40.02**	**−47 48 29.86**	**6**	**178**
1511-558	**15 15 12.67**	**−55 59 32.84**	**3**	**43**
1519-273	**15 22 37.68**	**−27 30 10.79**	**6**	**84**
1528-684	15 33 34.49	−68 37 19.65	2	27
1530-536	15 34 20.66	−53 51 13.42	2	19
1531-352	15 34 54.69	−35 26 23.50	1	40
1533-653	15 38 11.92	−65 25 51.20	2	7
1540-828	15 50 59.14	−82 58 6.85	2	62
1544-638	15 48 30.40	−64 1 34.80	3	57
1549-790	15 56 58.87	−79 14 4.28	4	17
1554-643	15 58 50.28	−64 32 29.64	15	92
1556-245	**15 59 41.41**	**−24 42 38.83**	**2**	**4**
1556-580	16 0 12.38	−58 11 2.97	1	6
1600-445	**16 4 31.02**	**−44 41 31.97**	**5**	**77**
1600-489	16 3 50.68	−49 4 5.51	1	13
1604-333	16 7 34.76	−33 31 8.91	13	79
1606-398	**16 10 21.88**	**−39 58 58.33**	**5**	**61**
1611-710	16 16 30.64	−71 8 31.45	18	178
1618-399	16 21 59.69	−40 3 34.49	1	4
1619-680	**16 24 18.44**	**−68 9 12.50**	**26**	**596**
1622-253	16 25 46.89	−25 27 38.33	1	6
1624-617	**16 28 54.69**	**−61 52 36.40**	**31**	**644**
1633-810	16 42 57.35	−81 8 35.07	14	125
1637-771	16 44 16.12	−77 15 48.81	1	10
1642-645	16 47 37.74	−64 38 0.27	2	59
1646-506	16 50 16.63	−50 44 48.21	7	68
1647-296	**16 50 39.54**	**−29 43 46.95**	**5**	**159**
1657-261	**17 0 53.15**	**−26 10 51.73**	**3**	**68**
1657-562	17 1 44.86	−56 21 55.90	25	495
1659-621	17 3 36.54	−62 12 40.01	27	572
1710-269	17 13 31.28	−26 58 52.53	1	21
1717-618	17 21 39.02	−61 54 43.02	1	3
1718-259	**17 21 55.98**	**−25 58 40.69**	**1**	**1**
1722-554	17 26 49.63	−55 29 40.46	1	3
1722-644	17 26 57.83	−64 27 52.71	2	8
1725-795	17 33 40.70	−79 35 55.72	19	257
1729-373	17 33 15.19	−37 22 32.40	2	10
1732-593	17 37 19.67	−59 21 41.89	1	6
1740-517	17 44 25.45	−51 44 43.74	5	25
1758-651	18 3 23.50	−65 7 36.76	20	378
1759-396	**18 2 42.68**	**−39 40 7.91**	**4**	**106**
1803-642	18 7 54.03	−64 13 50.11	4	104
1804-502	18 8 13.84	−50 11 53.61	2	52
1806-458	**18 9 57.87**	**−45 52 41.01**	**26**	**390**
1814-637	18 19 35.00	−63 45 48.21	1	9
1815-553	**18 19 45.40**	**−55 21 20.75**	**24**	**412**
1824-582	18 29 12.40	−58 13 55.16	19	319
1828-733	18 34 53.20	−73 15 14.33	3	9
1829-207	18 32 11.05	−20 39 48.20	1	4
1830-589	18 34 27.47	−58 56 36.27	1	8
1831-711	**18 37 28.71**	**−71 8 43.55**	**35**	**779**
1852-534	18 57 0.45	−53 25 0.38	2	10
1908-201	**19 11 9.65**	**−20 6 55.11**	**4**	**42**
1918-634	19 23 24.61	−63 20 45.77	1	2
1921-293	**19 24 51.06**	**−29 14 30.12**	**8**	**112**
1925-610	**19 30 6.16**	**−60 56 9.18**	**29**	**704**
1928-698	19 33 31.16	−69 42 58.91	6	136
1929-457	**19 32 44.89**	**−45 36 37.93**	**9**	**67**
1933-400	19 37 16.22	−39 58 1.55	20	541
1934-638	19 39 25.03	−63 42 45.62	2	6

https://doi.org/10.1017/pasa.2023.33 Published online by Cambridge University Press

1935-692	**19 40 25.53**	**−69 7 56.97**	**31**	**427**
1936-623	19 41 21.77	−62 11 21.06	7	193
1941-554	19 45 24.23	−55 20 48.84	1	5
1946-582	19 50 37.40	−58 4 39.75	1	2
1950-613	19 55 10.77	−61 15 19.14	6	66
1953-325	19 56 59.46	−32 25 46.01	1	11
1954-388	**19 57 59.82**	**−38 45 6.36**	**27**	**578**
1959-639	20 4 29.48	−63 47 23.31	4	95
2002-375	**20 5 55.07**	**−37 23 41.48**	**24**	**554**
2004-447	20 7 55.18	−44 34 44.28	1	7
2008-159	**20 11 15.71**	**−15 46 40.25**	**2**	**23**
2018-453	20 22 26.41	−45 13 29.55	2	36
2021-330	20 24 35.58	−32 53 35.91	1	43
2030-689	20 35 48.88	−68 46 33.84	5	147
2037-253	**20 40 8.77**	**−25 7 46.66**	**3**	**17**
2052-474	**20 56 16.36**	**−47 14 47.63**	**33**	**589**
2102-659	21 6 59.72	−65 47 43.59	6	44
2106-413	21 9 33.19	−41 10 20.61	18	329
2107-105	21 10 0.98	−10 20 57.32	1	9
2109-811	**21 16 30.85**	**−80 53 55.22**	**5**	**132**
2112-556	21 16 29.82	−55 27 20.44	1	17
2117-614	21 21 4.07	−61 11 24.62	4	29
2117-642	21 21 55.02	−64 4 30.04	1	1
2123-463	21 26 30.70	−46 5 47.89	21	311
2126-185	21 29 21.42	−18 21 22.79	1	24
2140-781	21 46 30.07	−77 55 54.73	1	25
2142-758	**21 47 12.73**	**−75 36 13.22**	**30**	**818**
2142-765	21 47 53.15	−76 21 29.22	1	9
2146-783	21 52 3.15	−78 7 6.64	9	139
2152-699	21 57 5.98	−69 41 23.68	1	22
2200-617	22 3 59.64	−61 30 22.01	1	33
2204-540	22 7 43.73	−53 46 33.82	30	557
2205-636	22 8 47.24	−63 25 47.49	1	1
2210-257	**22 13 2.50**	**−25 29 30.08**	**2**	**34**
2215-508	22 18 19.02	−50 38 41.73	1	13
2220-351	**22 23 5.93**	**−34 55 47.18**	**23**	**334**
2224-793	22 29 18.54	−79 7 8.52	1	24
2225-694	22 29 0.18	−69 10 30.27	1	27
2227-445	22 30 56.44	−44 16 29.89	3	74
2232-488	**22 35 13.24**	**−48 35 58.79**	**27**	**505**
2236-572	**22 39 12.08**	**−57 1 0.84**	**27**	**695**
2239-631	22 43 7.84	−62 50 57.32	1	19
2243-563	22 46 16.79	−56 7 46.01	3	44
2244-372	**22 47 3.92**	**−36 57 46.30**	**24**	**380**
2245-328	**22 48 38.69**	**−32 35 52.19**	**22**	**492**
2255-282	22 58 5.96	−27 58 21.26	1	14
2300-683	23 3 43.56	−68 7 37.44	21	316
2311-452	23 14 9.38	−44 55 49.24	1	12
2311-477	23 13 51.90	−47 29 11.73	1	3
2318-087	23 21 18.25	−8 27 21.52	1	6
2321-065	23 23 39.11	−6 17 59.24	1	4
2326-477	23 29 17.70	−47 30 19.11	25	443
2331-240	**23 33 55.24**	**−23 43 40.66**	**2**	**14**
2333-415	23 36 33.99	−41 15 21.98	24	276
2333-528	23 36 12.14	−52 36 21.95	7	131
2344-514	23 47 19.86	−51 10 36.07	20	279
2345-500	23 47 43.69	−49 46 27.88	1	5
2351-154	23 54 30.20	−15 13 11.21	1	8
2353-686	**23 56 0.68**	**−68 20 3.47**	**27**	**648**
2355-534	**23 57 53.27**	**−53 11 13.69**	**33**	**600**
2357-318	23 59 35.49	−31 33 43.82	20	308

Appendix 2. Session Summary Statistics for CRDS53-116

Table B.1 summarises the data set used for the overview of the CRDS network performance: the first column is the session code, column 2 is the start date of the session, column 3 is the number of IVS stations scheduled and in brackets the number that actually observed or provided usable data, column 4 is the number of scheduled observations in the session, column 5 is the number of observations that were able to be correlated, column 6 are the number of recoverable observations, column 7 are the number of observations actually used for the analysis, and column 8 is the post-fit residuals in picoseconds (ps) for the session.

Table B.1 Session summary statistics for CRDS53-116.

Session	Start date	Stations	Scheduled	Correlated	Recoverable	Obs	Fit
	YYYY.DOY	scheduled	Obs	Obs	Obs	used	ps
CRDS53	2011.222	5(5)	812	718	462	449	40.9
CRDS54	2011.278	4(3)	696	217	149	142	45.5
CRDS55	2011.320	5(4)	956	431	249	231	65.3
CRDS56	2012.016	3(3)	360	230	148	145	51.4
CRDS57	2012.032	3(3)	360	146	93	92	25.1
CRDS58	2012.131	3(3)	861	619	559	557	38.0
CRDS59	2012.143	3(3)	363	144	98	97	29.0
CRDS60	2012.207	4(3)	822	665	197	193	42.4
CRDS61	2012.256	5(5)	1087	1007	755	635	42.1
CRDS62	2012.333	5(4)	1100	450	282	272	68.4
CRDS63	2013.014	6(4)	1616	587	477	470	56.9
CRDS64	2013.084	4(4)	714	639	490	475	29.6
CRDS65	2013.128	6(5)	1616	786	371	353	38.3
CRDS66	2013.211	5(5)	1245	1115	778	771	35.6
CRDS67	2013.245	6(6)	1978	1680	1402	1382	38.0
CRDS68	2013.331	6(5)	1864	1116	826	810	36.5
CRDS69	2014.043	6(5)	1840	1444	756	711	27.0
CRDS70	2014.097	6(4)	1884	936	523	506	36.7
CRDS71	2014.177	6(6)	1915	1144	849	839	33.2
CRDS72	2014.233	6(6)	1911	1847	1438	1393	32.9
CRDS73	2014.279	6(6)	1914	1018	774	762	37.5
CRDS74	2014.343	6(6)	1850	1641	1243	1215	40.3

https://doi.org/10.1017/pasa.2023.33 Published online by Cambridge University Press

Table B.1 Continued.

Session	Start date YYYY.DOY	Stations scheduled	Scheduled Obs	Correlated Obs	Recoverable Obs	Obs used	Fit ps
CRDS75	2015.027	6(5)	1905	1245	821	820	40.4
CRDS76	2015.090	6(6)	1850	1728	1272	1247	25.1
CRDS77	2015.139	6(5)	1917	1180	704	632	40.0
CRDS78	2015.224	5(5)	1244	1208	922	921	18.8
CRDS79	2015.265	5(4)	1220	615	431	431	27.7
CRDS80	2015.285	5(4)	1403	610	425	425	13.4
CRDS81	2016.027	6(6)	2003	1740	1163	1161	34.9
CRDS82	2016.097	6(6)	2109	1992	1314	1312	31.1
CRDS83	2016.137	4(4)	846	751	442	442	23.7
CRDS84	2016.202	5(4)	1383	870	651	651	19.4
CRDS85	2016.271	6(6)	2089	1449	989	988	25.0
CRDS86	2016.328	6(5)	2101	1171	875	872	26.4
CRDS87	2017.094	6(6)	2092	1719	1214	1213	25.9
CRDS88	2017.137	5(4)	1362	707	531	531	23.4
CRDS89	2017.207	5(5)	1360	1335	984	984	38.1
CRDS90	2017.227	5(5)	1317	1259	872	852	37.2
CRDS91	2017.270	5(5)	1341	1203	897	866	33.0
CRDS92	2017.327	5(5)	1384	1369	937	905	37.0
CRDS93	2018.024	5(5)	1716	1653	696	644	79.8
CRDS96	2018.171	5(5)	1756	1667	995	914	31.4

Table B.1 Continued.

Session	Start date YYYY.DOY	Stations scheduled	Scheduled Obs	Correlated Obs	Recoverable Obs	Obs used	Fit ps
CRDS97	2018.226	5(5)	1779	1221	767	713	34.0
CRDS98	2018.269	5(5)	2140	2090	1458	1299	42.4
CRDS99	2019.015	5(4)	1386	620	365	340	47.2
CRD101	2019.086	5(5)	1711	1707	1245	1186	40.3
CRD102	2019.126	6(6)	2322	2264	1518	1422	33.6
CRD103	2019.176	6(6)	2386	1517	874	844	51.4
CRD104	2019.218	6(5)	2356	1482	738	719	34.5
CRD105	2020.036	6(6)	2480	2362	500	477	36.4
CRD106	2020.126	6(6)	2698	1468	550	527	52.2
CRD107	2020.203	6(6)	2585	1063	388	369	39.3
CRD108	2020.217	6(6)	2798	1369	333	303	36.9
CRD109	2020.331	6(6)	2259	1838	464	381	46.6
CRD110	2020.344	6(6)	2340	1592	441	432	46.8
CRD111	2021.033	5(5)	1611	1435	860	838	52.1
CRD112	2021.124	6(4)	1929	1038	923	910	23.4
CRD113	2021.208	6(5)	1913	1038	653	637	44.5
CRD114	2021.230	7(4)	1665	404	194	186	38.2
CRD115	2021.286	9(5)	1715	394	232	227	21.1
CRD116	2021.335	8(4)	1414	564	292	272	27.7

https://doi.org/10.1017/pasa.2023.33 Published online by Cambridge University Press